สารประกอบเชิงซ้อนของอนุพันธ์ 8-ไฮดรอกซีควิโนลีนเป็นตัวรับรู้ทางเคมีเรื่องแสงแบบเปิด

นายชาคริต ยิ้มสุขอนันต์

วิทยานิพนธ์นี้เป็นส่วนหนึ่งของการศึกษาตามหลักสูตรปริญญาวิทยาศาสตรมหาบัณฑิต
สาขาวิชาเคมี ภาควิชาเคมี
คณะวิทยาศาสตร์ จุฬาลงกรณ์มหาวิทยาลัย
ปีการศึกษา 2558
ลิขสิทธิ์ของจุฬาลงกรณ์มหาวิทยาลัย

COMPLEXES OF 8-HYDROXYQUINOLINE DERIVATIVES AS TURN-
ON FLUORESCENT CHEMOSENSOR

Mr. Chakrit Yimsukanan

A Thesis Submitted in Partial Fulfillment of the Requirements

for the Degree of Master of Science Program in Chemistry

Department of Chemistry

Faculty of Science

Chulalongkorn University

Academic Year 2015

Thesis Title	COMPLEXES OF 8-HYDROXYQUINOLINE DERIVATIVES AS TURN-ON FLUORESCENT CHEMOSENSOR
By	Mr. Chakrit Yimsukanan
Field of Study	Chemistry
Thesis Advisor	Professor Mongkol Sukwattanasinitt, Ph.D.
Thesis Co-Advisor	Associate Professor Paitoon Rashatasakhon, Ph.D.

Accepted by the Faculty of Science, Chulalongkorn University in Partial Fulfillment of the Requirements for the Master's Degree

⋯⋯⋯⋯⋯⋯⋯⋯⋯⋯⋯⋯⋯Dean of the Faculty of Science

(Associate Professor Polkit Sangvanich, Ph.D.)

THESIS COMMITTEE

⋯⋯⋯⋯⋯⋯⋯⋯⋯⋯⋯⋯⋯Chairman

(Associate Professor Vudhichai Parasuk, Ph.D.)

⋯⋯⋯⋯⋯⋯⋯⋯⋯⋯⋯⋯⋯Thesis Advisor

(Professor Mongkol Sukwattanasinitt, Ph.D.)

⋯⋯⋯⋯⋯⋯⋯⋯⋯⋯⋯⋯⋯Thesis Co-Advisor

(Associate Professor Paitoon Rashatasakhon, Ph.D.)

⋯⋯⋯⋯⋯⋯⋯⋯⋯⋯⋯⋯⋯Examiner

(Assistant Professor Anawat Ajavakom, Ph.D.)

⋯⋯⋯⋯⋯⋯⋯⋯⋯⋯⋯⋯⋯External Examiner

(Nakorn Niamnont, Ph.D.)

ชาคริต ยิ้มสุขอนันต์ : สารประกอบเชิงซ้อนของอนุพันธ์ 8-ไฮดรอกซีควิโนลีนเป็นตัวรับรู้ทางเคมีเรื่องแสงแบบเปิด (COMPLEXES OF 8-HYDROXYQUINOLINE DERIVATIVES AS TURN-ON FLUORESCENT CHEMOSENSOR) อ.ที่ปรึกษาวิทยานิพนธ์หลัก: ศ. ดร.มงคล สุขวัฒนาสินิทธิ์, อ.ที่ปรึกษาวิทยานิพนธ์ร่วม: รศ. ดร.ไพฑูรย์ รัชตะสาคร, 50 หน้า.

ในปัจจุบันตัวตรวจวัดทางเคมีที่ใช้หลักการฟลูออเรสเซนต์มีบทบาทสำคัญในการนำใช้เป็นเทคนิคการตรวจวัดในด้านทางเคมี ทางชีววิทยา และทางด้านสิ่งแวดล้อม ซึ่งรวมไปถึงตรวจวัดไอออนของโลหะ โดยในงานวิทยานิพนธ์ชิ้นนี้ได้พัฒนาตัวตรวจวัดไอออนของโลหะแบบเปล่งแสงจาก 8-ไฮดรอกซีควิโนลีน (8HQ) ซึ่งอนุพันธ์ของ 8-ไฮดรอกซีควิโนลีนชนิดใหม่ทั้งสาม (Q1, Q2 และ Q3) จะมีโครงสร้างดังนี้ โดยสาร Q1 จะมีโครงสร้างของ 8HQ ที่แทนที่ O ด้วยสายเอทิลีนไกลซิล อะซิเตตเอสเตอร์ การแทนที่ O ด้วยสายเอทิลีนไกลคอลและเพิ่มระบบไพคอนจูเกชั่นที่ตำแหน่งที่ 5 ด้วย 4-เอทินิลไดเมทิลอะนิลีนได้สาร Q2 และการเพิ่มหมู่อะซิทิลที่ปลายสารไกลคอลได้สาร Q3 ในตัวทำละลายอะซีโตไนไตรล์ สเปกตรัมการดูดกลืนแสงของ 8HQ และ Q1 ที่คล้ายกันคือ มีค่าการดูดกลืนสูงสุดที่ความยาวคลื่น 240 และ 300 นาโนเมตร ในขณะที่สารอีกสองชนิด Q2 และ Q3 มีการดูดกลืนเหมือนกันที่ความยาวคลื่น 300 และ 370 นาโนเมตร ซึ่งค่าการคายแสงของสาร 8HQ และ Q1 คายที่ความยาวคลื่น 400 นาโนเมตร ในขณะที่สาร Q2 และ Q3 การคายแสงจะเลื่อนไปที่ 560 นาโนเมตร ในตัวทำละลายโพลาร์อะโปรติกการเรืองแสงของสาร Q2 และ Q3 จะสามารถมองเห็นได้ภายใต้แสง black light แต่จะไม่มีการเรืองแสงในตัวทำละลายโพลาร์โปรติก เช่น เมทานอล หรือน้ำ ซึ่งการดับสัญญาณการเรืองแสงในตัวทำละลายดังกล่าวเกิดขึ้นจากการเกิดพันธะไฮโดรเจนระหว่างตัวทำละลายกับหสารเรืองแสง ดังนั้นสารประกอบ 8HQ และอนุพันธ์ทั้งสามชนิดจะถูกนำไปตรวจวัดไอออนโลหะในตัวทำละลายผสม โดยในตัวทำละลายอะซิโตไนไตรล์/น้ำ (อัตราส่วน 90/10 โดยปริมาตร) มีเฉพาะสาร Q1 ที่แสดงการเปล่งแสงฟลูออเรสเซนต์แบบจำเพาะกับไอออนของไลหะประจุสามบวกได้แก่ Al^{3+}, Cr^{3+} และ Fe^{3+} ในขณะที่สาร 8HQ, Q2 และ Q3 ไม่แสดงการการเปลี่ยนแปลงสัญญาณฟลูออเรสเซนต์กับโลหะชนิดใด ในตัวทำละลายเมทานอล/น้ำ (อัตราส่วน 30/70 โดยปริมาตร) สาร 8HQ แสดงการเปล่งแสงฟลูออเรสเซนต์สีเขียวเมื่อเจอกับโลหะ Al^{3+} ในขณะที่สาร Q3 ได้เปล่งแสงฟลูออเรสเซนต์สีเขียว (ความยาวคลื่น 510 นาโนเมตร) อย่างจำเพาะเจาะจงกับโลหะ Hg^{2+} ให้ค่าต่ำสุดที่สามารถตรวจวัดได้ (LOD) กับ Hg^{2+} คือ 64 นาโนโมลาร์ หรือ 13 ส่วนในพันล้านส่วน (ppb) ปรากฏการณ์การเกิด Tyndall พร้อม ๆ กับการเพิ่มสัญญาณฟลูออเรสเซนต์เมื่อเติมโลหะ Hg^{2+} เพิ่มขึ้นทำให้พิจารณาได้ว่าการเพิ่มขึ้นของสัญญาณฟลูออเรสเซนต์ใน Q3 กับ Hg^{2+} เกิดจากปรากฏการณ์ aggregation induced emission (AIE) :เช่นเดียวกับการเพิ่มปริมาณสัดส่วนปริมาณของน้ำ (80-90%) ในตัวทำละลายของสาร Q3 ที่ไม่มีโลหะ Hg^{2+} จะพบปรากฏการณ์การเกิด AIE

ภาควิชา	เคมี	ลายมือชื่อนิสิต	....
สาขาวิชา	เคมี	ลายมือชื่อ อ.ที่ปรึกษาหลัก	....
ปีการศึกษา	2558	ลายมือชื่อ อ.ที่ปรึกษาร่วม	....

5571955923 : MAJOR CHEMISTRY

KEYWORDS: Fluorescence Sensor / MERCURY SENSOR / AGGREGATION-INDUCED EMISSION ENHANCEMENT (AIEE) / HYDROXYQUINOLINE

CHAKRIT YIMSUKANAN: COMPLEXES OF 8-HYDROXYQUINOLINE DERIVATIVES AS TURN-ON FLUORESCENT CHEMOSENSOR. ADVISOR: PROF. MONGKOL SUKWATTANASINITT, Ph.D., CO-ADVISOR: ASSOC. PROF. PAITOON RASHATASAKHON, Ph.D., 50 pp.

Nowadays, fluorescent chemosensors play an important role in detection method in chemical, biological, and environmental fields, including detection of metal ions. In this work, turn-on fluorescent sensors for metal ions are developed from 8-hydroxyquinoline (8HQ). Three new 8-hydroxyquinoline derivatives (Q1, Q2 and Q3) are synthesized. For Q1, 8HO is O-substituted with acetate ester of diethylene glycol. The O-substitution of 8HQ with diethylene glycol followed by the extension of the pi-conjugation at 5-position with 4-ethynyl N,N-dimethyl aniline moiety gives Q2 and the acetylation of Q2 gives Q3. In CH_3CN, the absorption spectra of 8HQ and Q1 are similar showing two absorption maxima around 240 and 300 nm, while those of Q2 and Q3 are around 300 and 370 nm. The emission maximum of 8HQ and Q1 is observed at 400 nm whereas that of Q2 and Q3 is red-shifted to 560 nm. In polar aprotic solvent, the fluorescence of Q2 and Q3 are visible to naked-eye under black light that become invisible in protic solvents such as CH_3OH and H_2O. The fluorescence quenching in protic solvents is probably associated with the hydrogen bonding between the solvents and fluorophores. Therefore, 8HQ and its derivatives are investigated as turn-on fluorescent sensors for metal ions in mixed solvents. In CH_3CN/H_2O (90/10 v/v), only Q1 shows selective turn-on fluorescence with trivalent ions such as Al^{3+} Cr^{3+} and Fe^{3+}, while 8HQ, Q2 and Q3 show non-selective and low fluorescence response to metal ions. In CH_3OH/H_2O (30/70 v/v), 8HQ show known green fluorescence enhancement with Al^{3+} while Q3 shows interestingly strong green fluorescence (510 nm) enhancement selectively with Hg^{2+}. The detection limit of Hg^{2+} by Q3 is 64 nM or 13 ppb. The Tyndall effect observed along with the increase of fluorescence intensity of Q3 upon the addition of Hg^{2+} suggests that the fluorescence enhancement of Q3 with Hg^{2+} is due to the aggregation induced emission (AIE). The AIE of Q3 is also observed without Hg^{2+} at higher fraction of H_2O (80-90%).

Department:	Chemistry	Student's Signature	....
Field of Study:	Chemistry	Advisor's Signature	....
Academic Year:	2015	Co-Advisor's Signature	....

ACKNOWLEDGEMENTS

CONTENTS

LIST OF FIGURES

LIST OF TABLES

CHAPTER I

INTRODUCTION

1.1 Fluorescent chemosensors

Nowadays, fluorescent chemosensors play an important role in detection method in chemical, biological, and environmental fields, including detection of metal ion, anion, neutral molecules and biomolecules. Fluorescent technique has significant advantages over other methods such as high selectivity, high sensitivity, short response time, cost-effectiveness in instrumentation, operational simplicity, and also no destruction of samples. Most of the fluorescent chemosensors are composed of two main components: one is a receptor unit for selective binding of the analytes, the other is a fluorophore unit provides the means of signaling this bonding, whether by fluorescence quenching, enhancement or wavelength shift. The photophysical signaling mechanisms which controls the response of a fluorophore to analytes binding include photoinduced electron transfer (PET) [1-7], intramolecular charge transfer (ICT) [2-7], Förster resonance energy transfer (FRET) [8, 9], excited-state intramolecular proton transfer (ESIPT) [10, 11], Isomerization [12], aggregation-induced enhancement fluorescence (AIE) [13, 14], aggregation-caused quenching (ACQ), and excimer/exciplex formation [2-4, 7, 15]. In addition, a chemosensor may be designed by using more than one sensing mechanism in order to enhance response of signal transduction.

a) Fluorescence turn-off

b) Fluorescence turn-on

c) Wavelength shift
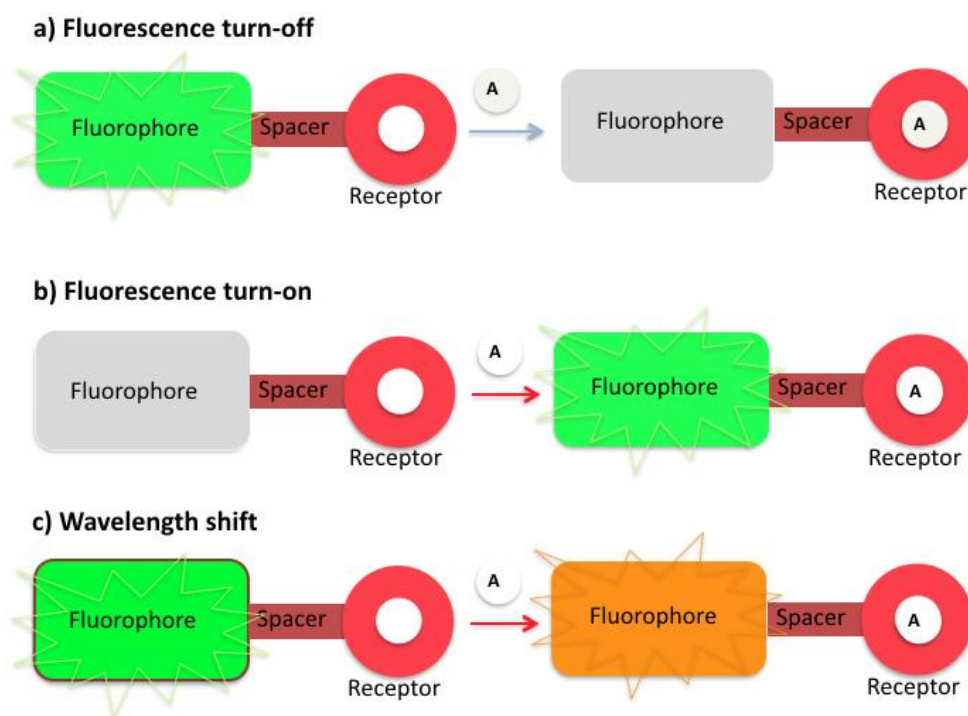
Figure 1.1 Changes of fluorescent signal.

1.2 Fluorescence

Fluorescence is the emission of light typically occurring with aromatic compounds or highly conjugated molecules. The fluorescence processes that occur between the absorption and emission of light can be usually described by the Jablonski diagram as shown in Figure 1.2 [16]. Upon the absorption of light energy, the molecule is excited to excited states (S_1 or S_2) and forms an excited molecule. The molecule rapidly relaxes to the lowest vibrational level of S_1 which this process is called internal conversion. The final process, the molecule returns to ground state (S_0) via emission of a longer wavelength photon. The time required to complete this process takes nano-second.
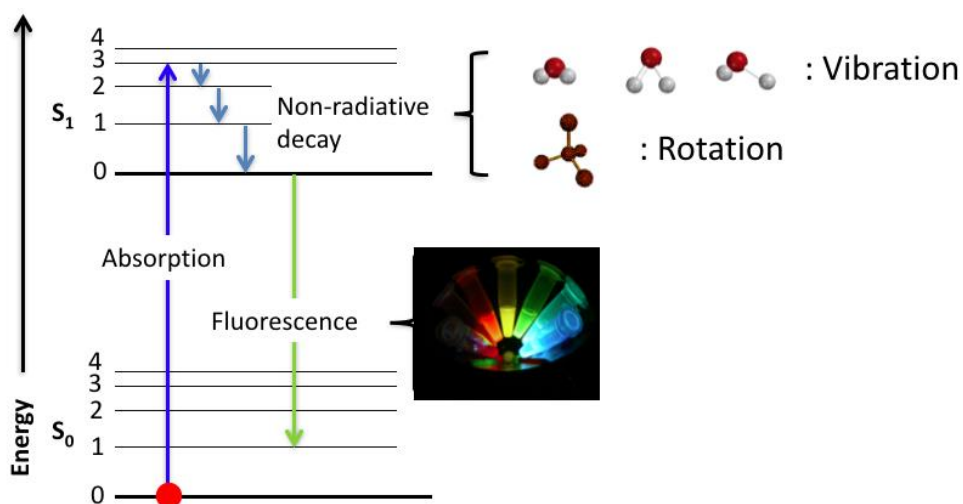
Figure 1.2 Simple Jablonski diagram illustrating fluorescent processes. [16]

1.3 Sensing mechanisms

1.3.1 Photoinduced electron transfer (PET)

PET process can occur when receptor or analyte has either its highest occupied molecular orbital (HOMO) (Donor) or the lowest unoccupied molecular orbital (LUMO) (acceptor) level between HOMO and LUMO gap of the fluorophore. In the first case, an electron of fluorophore is excited to its LUMO level. A HOMO electron of the donor presumably transfers to the HOMO level of the excited fluorophore which acts as the electron acceptor. After that, the excited electron in LUMO level can transfer to the HOMO level of the donor (Figure 1.3, left). In the latter case, the excited electron in LUMO level of the fluorophore transfer to the LUMO level of the acceptor before transferring back to the half-filled HOMO level of the fluorophore (Figure 1.3, right). In this case, the excited fluorophore acts as the electron donor. The electron transfer process is a non-radiative process which results in quenching of the fluorescence.
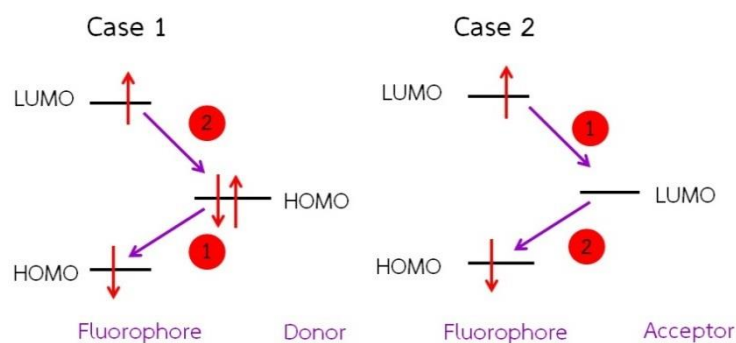
Figure 1.3 Principal photophysics of PET.

1.3.2 Excited state intramolecular proton transfer (ESIPT)

The ESIPT process generally associates with the transfer of a proton of a hydroxyl (or amino) group to a carbonyl oxygen (or imine nitrogen) through a pre-existing six- or five-membered ring hydrogen bonding configuration [17]. The classic example of the ESIPT photophysical process was observed for 2-(20-hydroxyphenyl)-benzoxazole (HBO) as illustrated in Figure. 1.4. After irradiation, the HBO in enol form (E*) is converted to the excited-state keto form (K) in the sub picosecond time scale resulting in significantly red shift emission compared with the absorption and unusually large Stoke shift. A large Stoke shift is beneficial in fluorescence sensing to avoid the self-absorption or the inner filter effect.
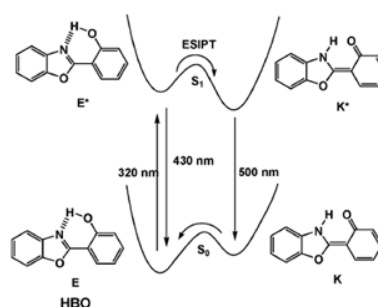
Figure 1.4 Principal photophysics of ESIPT. Illustrated by 2-(20-hydroxyphenyl)-benzoxazole (HBO). [17]

1.3.3 Intramolecular charge transfer (ICT)

The initial most stable excited state of S_1 is sometime called locally excited)LE (state .In certain cases, a molecule in LE state may undergoes another geometrical relaxation along with redistribution of electron density, especially when the molecule contains both electron donating and withdrawing groups connected via π-conjugated system .The relaxation process generates a new lower energy excited state called internal charge transfer)ICT (state having very different geometry and dipole moment from the LE state)Figure 1.5 .(The ICT state can then relax to the ground state either by radiative or non-radiative decay .Depending on the energy band gap, this relaxation may give light within or outside the visible light spectrum .[18-20] If detectable, this emission from the ICT state is at a longer wavelength and enhanced by polar solvent as the ICT excited state more populated by the solvent stabilization .Due to multistep process, ICT emission usually has lower fluorescence quantum yield compared with LE state .A "turn off "or "turn on "or "wavelength shift "fluorescent sensor can be designed based on the degree of the ICT process.
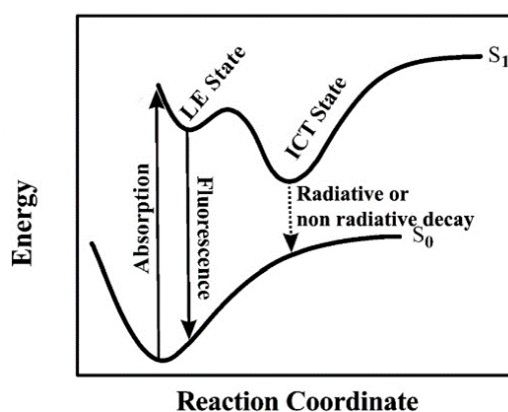
Figure 1.5 Potential energy surfaces of the ground state, S_0 is excited to S_1 then relaxed to LE, and ICT state.

1.3.4 The FÖrster resonance energy transfer (FRET)

The FÖrster resonance energy transfer)FRET (between two molecules is an important photophysical phenomenon applied in studying biological systems and biomedical research .FRET occurs when the emission spectrum of a donor fluorophore)D (overlaps with the absorption spectrum of acceptor fluorophore)A ((Figure 1.7 .(FRET is not the result of emission from the donor being absorbed by the acceptor .There is no intermediate photon in FRET .The mechanism is D in an excited electronic state, which transfer its excitation energy to a nearby A in nonradiative decay through long range dipole-dipole interactions .The supporting theory is based on the idea of an oscillating dipole that can undergo an energy exchange with a second dipole which has a similar resonance frequency .Also, resonance energy transfer is similar behavior of coupled oscillators .FRET is highly distance dependent, it is thus one of few tools available as "spectroscopic ruler "for measuring nanometer scale distances and the changes in distances, both in vitro and in vivo, such as measurements of distance between active sites on a protein that has been labelled with donor-acceptor fluorophores .Also, a turn off fluorescent sensor or a shift of wavelength can be designed based on FRET process.
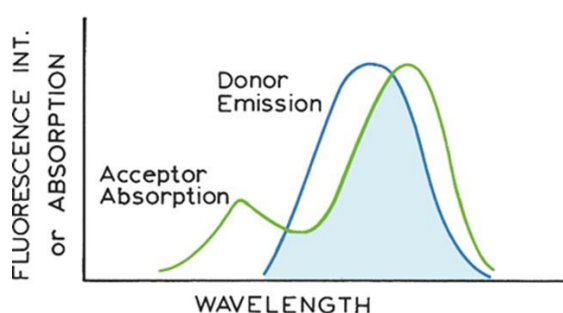
Figure 1.6 Spectral overlap for fluorescence resonance energy transfer, FRET [21].

1.3.5 Aggregation-induced emission (AIE)

Generally, aggregation of fluorophores is unwanted as it causes decreasing in emission by excimer formation. But some type of fluorophores exhibits highly fluorescent emission when aggregated in concentrated solutions or in solid state, while exhibits low fluoescence in dilute solutions. These fluorophores, such as Hexaphenylsilole, have shared characteristic of being propeller-shaped non-planar molecule. This property prevents formation of excimer by aggregation, and also enhances emission by restricts intramolecular rotations, which is non-radiative relaxation. This process was termed "aggregation-induced emission" (AIE) since aggregation leads to enhanced emission.
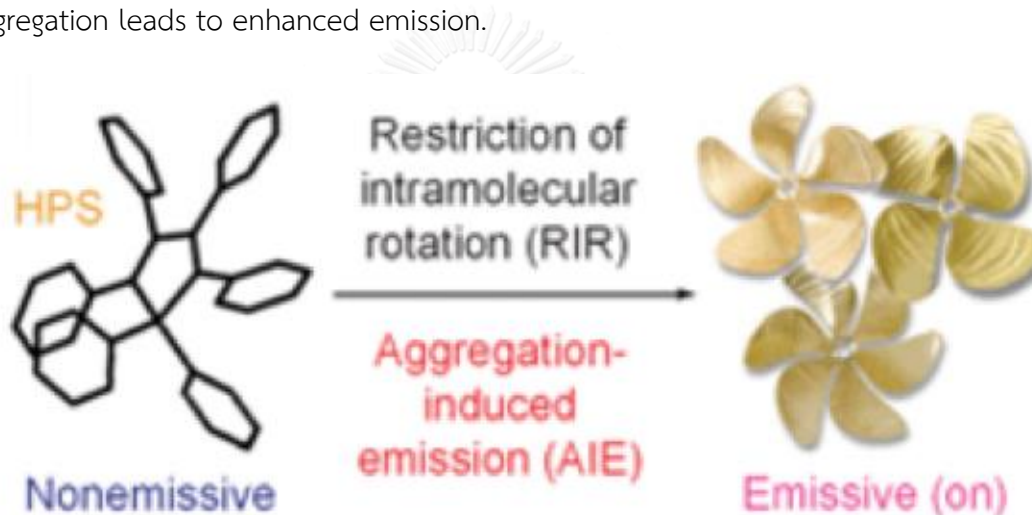
Figure 1.7 Principal photophysics of AIE. [22]

1.4 Mercury ions

Mercury is one of the most toxic metals and widespread in the food, water and soil that generated by various sources such as chemical plants, coal-fired power plants and environmental contaminant in food chain [23]. The extreme toxicity of mercury and its derivatives results from their high affinity for thiols in proteins and enzymes, leading to the dysfunction of cells [24]. Mercury can damage human heart, kidney stomach, brain and nervous system [25]. The World Health Organization (WHO) has limited the maximum allowable level of mercury ions of 1 ppb in drinking water. Therefore, the effective detection method for mercury is a great importance.

1.5 Fluorescence sensors for Hg^{2+}

Recently, the fluorescent chemosensors were widely used for mercury ions detection because it provided quick, nondestructive and highly sensitive advantages. It was also applicable for naked eye detection and on-site analysis. However, many of the reported [26-32] were based on "turn-off" fluorescence responses for mercury ions due to mercury's propensity to enhanced spin-orbit coupling by external heavy atom effect [33]. Consequently, the development of sensitive and selective "turn-on" fluorescence sensor for mercury ions is interesting and challenging. Fluorescence sensing mechanisms used in Hg^{2+} sensing are based on photophysical processes such as photoinduced electron transfer (PET) [34], intramolecular charge transfer (ICT) [35], and fluorescence resonance energy transfer (FRET) [36]. Recently, aggregation-induced emission (AIE) has also been introduced as a novel mechanism for "turn-on" fluorescence signal transduction in Hg^{2+} sensor [37].
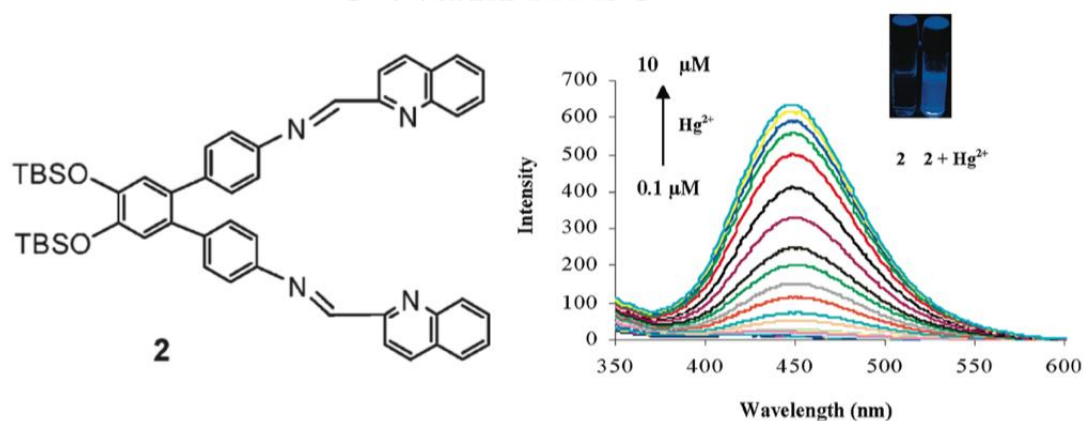
*Figure 1.8 (left) Structure of terphenyl-based receptor **2**. (right) Fluorescence titration of **2** upon addition of Hg^{2+}.*

In 2009, Bhalla et al. [34] synthesized a new terphenyl-based receptor with pyrene and quinoline as the fluorophores. Compound **2** showed the highly selective and sensitive "off-on" fluorescence signaling behavior for Hg^{2+} ions in THF and mixed aqueous media (THF:H_2O, 9.5:0.5).
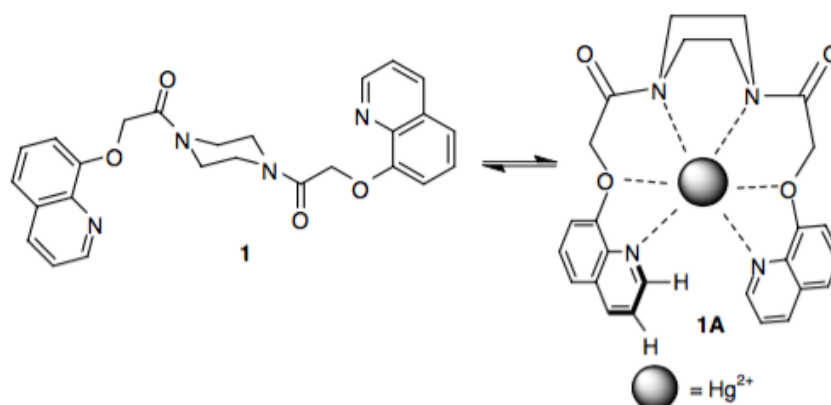
*Figure 1.9 Structure of **1** and proposed binding model of Hg^{2+} ion*

In 2013, Ghosh et al. [35] synthesized a chemosensor **1** from 8-hydroxyquinoline. Compound **1** recognises Hg^{2+} ions (K_a = 2.15 x 10^4 M^{-1}) by exhibiting ratiometric change in emission in $CHCl_3$/CH_3OH (1:1, v/v), under similar condition both Zn^{2+} and Cd^{2+} ions are sensed by significant non-ratiometric increase in emission with measurable red shift. In $DMSO$/H_2O (5:95, v/v), the sensor **1** exhibited a greater selectivity towards Hg^{2+} ions (Ka = 9.20 x 10^3 M^{-1}) over the other metal ions.
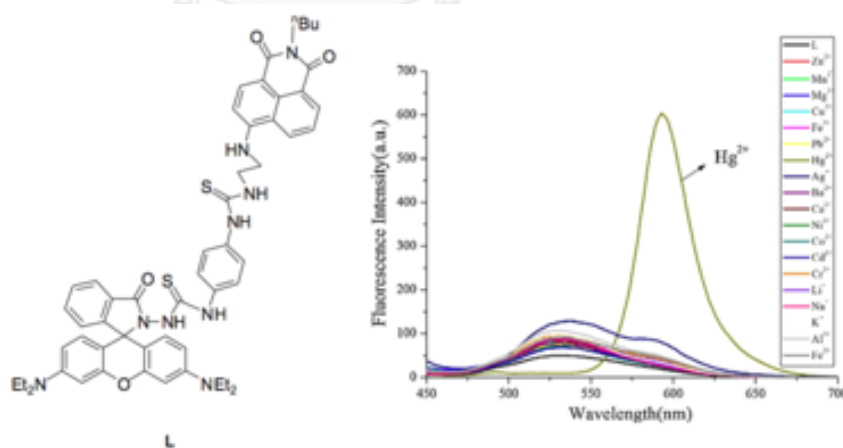
*Figure 1.10 (left) Structure of **L**. (right) Fluorescence spectra of **L** in presence of 10 eq. different metal ions in (1:2, v/v) MeOH/water solution (1 mM Tris–HCl, pH 7.0)*

In 2004, Wang et al. [36] synthesized a new ratiometric chemosensor based on rhodamine and naphthalimide fluorophore, **L** was synthesized and characterized. Compound **L** exhibited high selectivity and excellent sensitivity in both absorbance and fluorescence detection of Hg^{2+} in aqueous solution with a broad pH span (1–10). The coordination of **L** with Hg^{2+} was chemically and partially reversible. The significant changes in the fluorescence color could be used for naked-eye detection. Furthermore, fluorescence imaging experiments of Hg^{2+} in living EC 109 cells demonstrated its value of practical applications in biological systems.
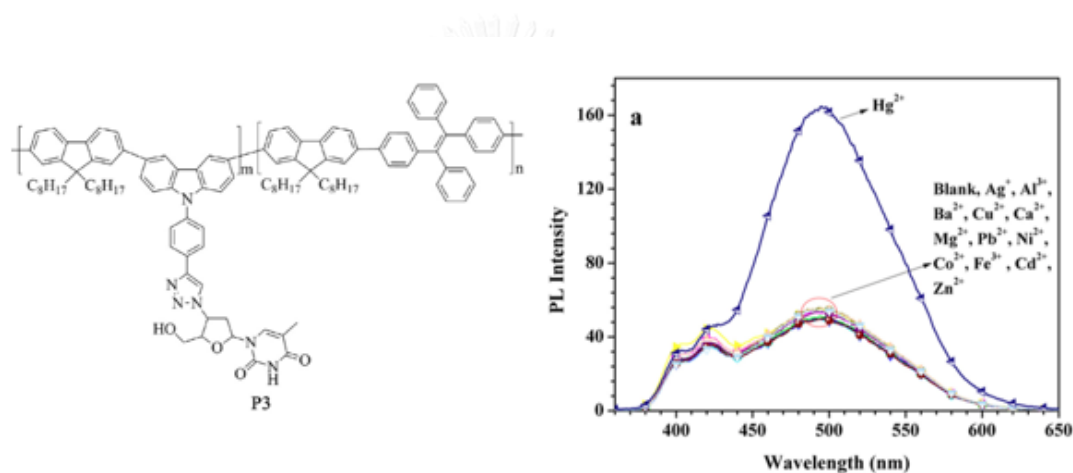
*Figure 1.11 (left) Structure of **P3**. (right) Fluorescence spectra of **P3** (1.5×10–5M) with the presence of various metal ions (0.1M) in THF–water mixture (V_{THF}/V_{water} =7/3) (buffered with citric acid-disodium hydrogen phosphate, 5 mM, pH = 7.4)*

In 2014, Sun et al. [37] synthesized a thymine (T)-covalently conjugated polymer (**P3**). With the introduction of aqueous Hg^{2+}, fluorescence of P3 in THF–water mixture (V_{THF}/V_{water} =7/3) (buffered with 5 mM citric acid–disodium hydrogen phosphate, pH = 7.4) displayed gradual enhancement. The AIEE effect was activated by the formation of intermolecular aggregates, which was induced by the formation of T–Hg–T complex between polymer chains. Other common metal ions brought very slight interference for **P3**'s response of Hg^{2+}, and the detection limit of Hg^{2+} reached ～15.3 nM for such probing system.

1.6 Fluorescence sensors based on 8-hydroxyquinoline

8-hydroxyquinoline (8HQ) is one of the most important chelating agents for metal ions such as Al^{3+}, Fe^{3+}, Cu^{2+}, Zn^{2+} and Cd^{2+} [38]. Several of these metal complexes of 8HQ possess high fluorescence thermal and photo-stability that makes them becomes one of the most widely studied emissive materials for organic light emitting diode (OLED) [39]. Interestingly, these metal complexes are more fluorescent in their solid state than in the solution as the results of the AIE effect. However, this interesting phenomenon of 8HQ complexes has not been seriously investigated for sensing application. Some examples of literature related to 8-hydroxyquinoline ions are as following:
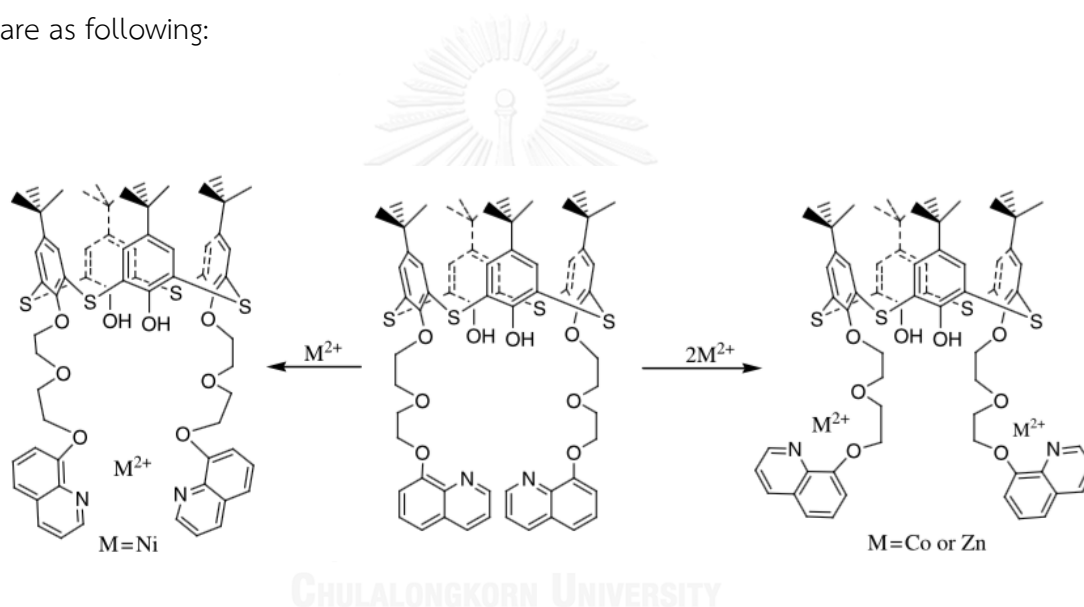
Figure 1.12 Proposed structures of the complexes of 1 with Ni²⁺, Co²⁺ and Zn²⁺

In 2006, Zhang et al. [40] synthesized a novel conic thiacalix[4]arene derivative (**1**) with diagonal quinolin-8-yloxy pendants via oxyethylene spacer has been synthesized in one step. The coordination properties of the new ligand towards Ni^{2+}, Co^{2+} and Zn^{2+} ions were studied by UV–vis, fluorescent spectra and ^{1}H NMR titration. The results showed that **1** formed very stable complexes with the three metal ions.
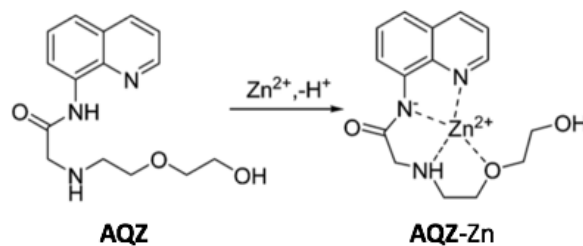
*Figure 1.13 Proposed structures of the complexes of **AQZ** with Zn^{2+}*

In 2008, Zhang et al. [41] synthesized a novel "naked-eye" and ratiometric fluorescent zinc sensor (**AQZ**) of carboxamidoquinoline with an alkoxyethylamino chain as receptor. **AQZ** shows good water solubility and high selectivity for sensing; about an 8-fold increase in fluorescence quantum yield and a 75 nm red-shift of fluorescence emission upon binding Zn^{2+} in buffer aqueous solution are observed. Moreover, AQZ can enter yeast cells and signal the presence of Zn^{2+}.
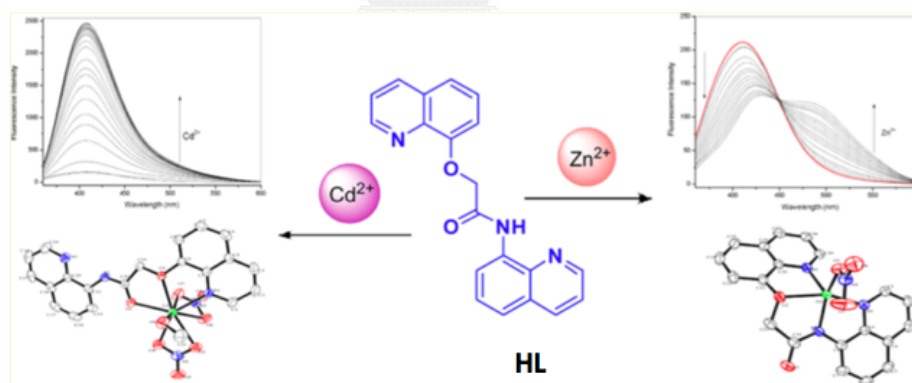
*Figure 1.14 Proposed structures of the complexes of **HL** with Cd^{2+} and Zn^{2+} and fluorescence titration spectra of these complexes*

In 2012, Zhou et al. [42] synthesized a fluorescent sensor **HL** based on 8-amino quinoline and 8-hydroxyquinoline **HL** displays high selectivity and sensitive fluorescence enhancement to Cd^{2+} in ethanol. Moreover, sensor **HL** can distinguish Cd^{2+} from Zn^{2+} via two different sensing mechanisms (photoinduced electron transfer

for Cd^{2+}; internal charge transfers for Zn^{2+}). The composition of the complex Cd^{2+}/**HL** or Zn^{2+}/L^- has been found to be 1:1, based on the fluorescence/absorption titration and further confirmed by X-ray crystallography.
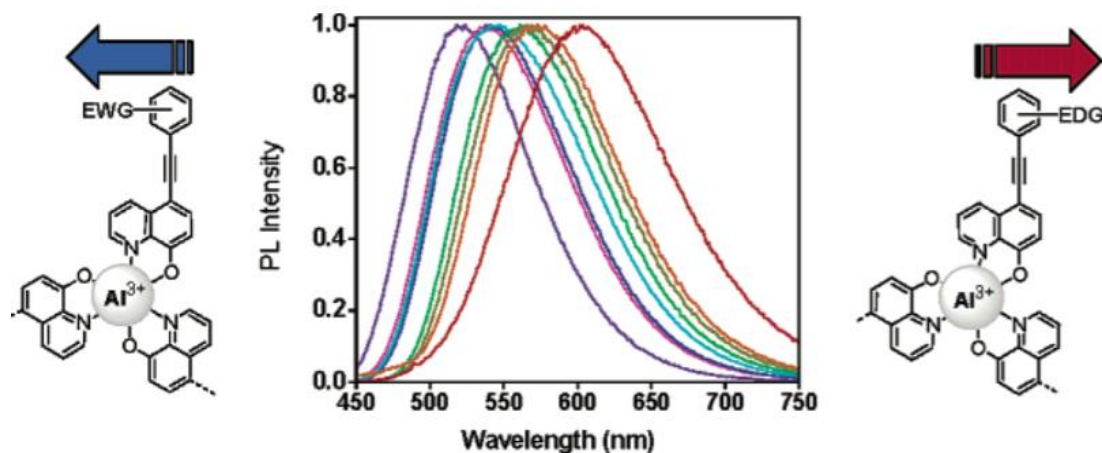
Figure 1.15 Fluorescence spectra of 5-arylethynyl-8-hydroxyquinoline derivatives

In 2003, Anzenbacher Jr. et al. [43] synthesized 5-arylethynyl-8-hydroxyquinoline derivatives using Sonogashira–Hagihara coupling The electronic nature of arylethynyl substituents affects the emission color and quantum yield of the resulting Al(III) complex. Photophysical properties of the metallocomplexes correspond to the electron-withdrawing/-donating character of the arylethynyl substituents. Optical properties of such Al(III) complexes correlate with the Hammett constant values of the respective substituents. This strategy offers a powerful tool for the preparation of electroluminophores with predictable photophysical properties.

1.7 Objectives of this research

The aim of this work designed and synthesized a novel series of three 8-hydroxyquinoline derivatives which having an ethylene glycol side-chain and extended π-conjugation of aromatic system (Figure 1.16). We expected that the ethylene glycol side-chain was incorporated to increase the binding heteroatoms for improved sensing properties. The incorporation of extended π-conjugation with the dimethylamino

electron donating group gives further modulation of the electronic properties of the fluorescence probes.
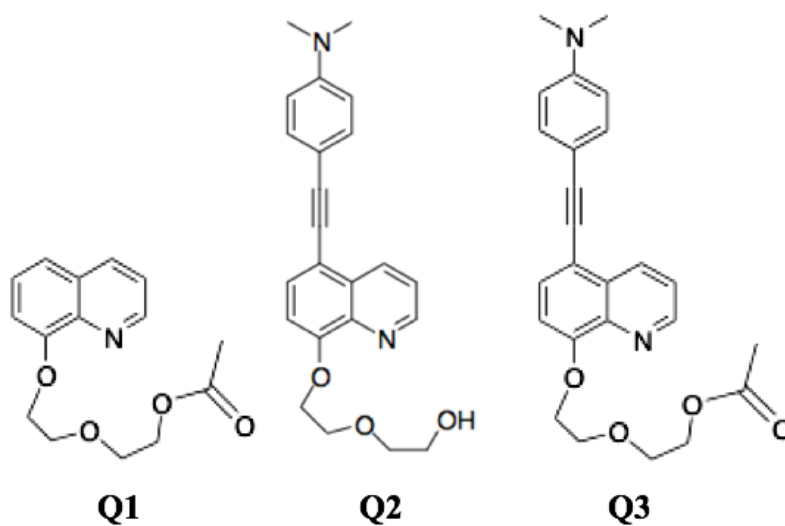
Figure 1.16 Target molecules **Q1-Q3**
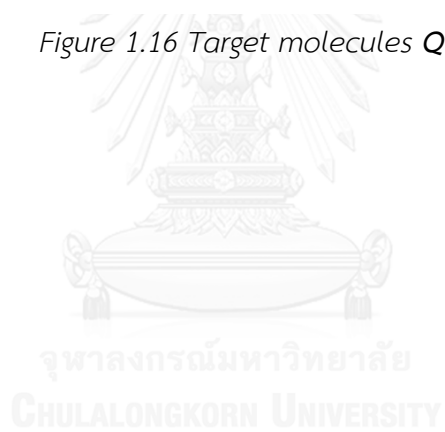
CHAPTER II

EXPERIMENT

2.1 Chemicals and materials

N,N-dimethylaniline trimethylsilylacetylene, copper (I) iodide , potassium carbonate, Palladium(II)dichloride ($PdCl_2$), potassium carbonate, calcium carbonate, and bovine serum albumin (BSA) were purchased from Fluka (Switzerland). diethylenegylcol, Tosyl chloride, tetrakis(triphenylphosphine) palladium(0), Triphenylamine, iodine monochloride, 1,8-diazabicyclo [5.4.0] undec-7-ene (DBU) and quinine sulfate were purchased from Aldrich. 8-hydroxyquinoline and 5-bromo-8-hydroxyquinoline, were purchased from TCI (Japan). All other reagents were non-selectively purchased from Sigma-Aldrich, Fluka or Merck (Germany). For most reactions, solvents such as dichloromethane and acetonitrile were reagent grade stored over molecular sieves. All column chromatography were operated using Merck silica gel 60 (70-230 mesh). Thin layer chromatography (TLC) was performed on silica gel plates (Merck F_{245}). Solvents used for extraction and chromatography such as dichloromethane, hexane, ethyl acetate and methanol were commercial grade. Milli-Q water was used in all experiments unless specified otherwise. The most reactions were carried out under positive pressure of N_2 filled in rubber balloons.

2.2 Analytical instruments

All ^{1}H NMR and ^{13}C NMR spectra were acquired on a Varian Mercury and Bruker 400 MHz NMR spectrometer, which operated at 400 MHz for ^{1}H and 100 MHz for ^{13}C nuclei. Mass spectra were recorded on a Microflex MALDI-TOF (Bruker Daltonics) using doubly recrystallized a-cyano-4-hydroxy cinnamic acid (CCA) and dithranol as a matrix. Absorption spectra were recorded using Shimadzu UV-2550 UV-vis spectro-photometer. Fluorescence measurements were performed in a quartz cuvette with 1.0 cm path length on a Varian Cary Eclipse spectrofluorometer with a xenon lamp as the excitation source. Fluorescent quantum yields were deter-mined by a relative method

using a quinine sulfate in 0.1 M H_2SO_4 (Φ_F = 0.54) as a reference. All of the measure-ments were performed at room temperature unless otherwise stated. The fluorescence response was determined as a ratio between the fluorescence intensity of the fluorophore in presence (I) and absence (I_0) of the analyst.

2.3 Synthesis of fluorophores

2.3.1 Synthesis of Q1

- Synthesis of compound 1
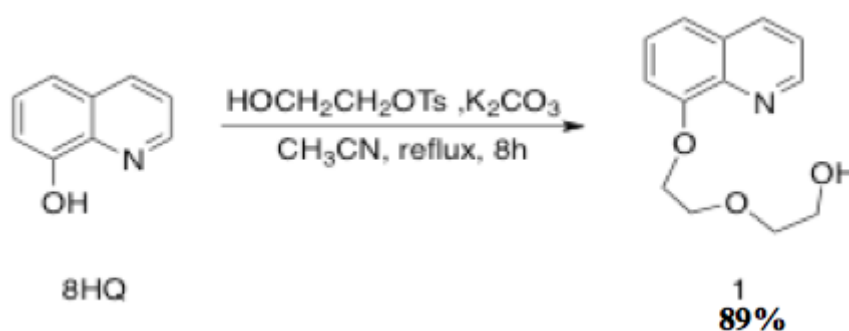
8-hydroxyquinoline (290 mg, 2 mmol) and potassium carbonate (2,488 mg, 6 mmol) was stirred to dissolve in acetonitrile (5 mL). Dietyleneglycol monotorsylate (520 mg, 2 mmol) was added dropwise to this stirred solution. After reflux within 8 hours of stirring, the mixture was removed under reduced pressure. The yellow solid residue was dissolved in dichloromethane (20 mL) and then extracted with water (2 × 20 mL). The organic layer was dried over anhydrous $MgSO_4$ and the solvent was removed under reduced pressure. The obtained crude product was further purified by silica gel column chromatography using dichloromethane/ethyl acetate (7:3 v/v) mixture as the eluent to afford 1 (415 mg, 89% yield). ^{1}H NMR (400 MHz, $CDCl_3$) δ 8.87 (d, J = 2.6 Hz, 1H), 8.11 (dd, J = 8.3, 1.3 Hz, 1H), 7.50 − 7.30 (m, 3H), 7.03 (d, J = 6.7 Hz, 1H), 4.32 (t, 2H), 4.24 (s, 1H), 4.05 (t, 2H), 3.82 (t, 2H), 3.73 (t, 2H).

- Synthesis of compound **Q1**
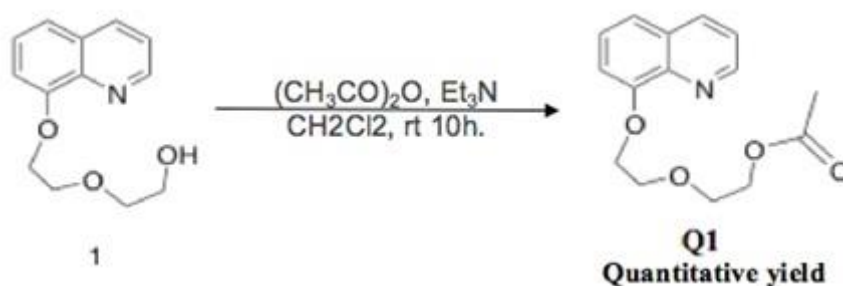
Compound **1** was acetylated by stirring a solution of **1** (500 mg, 2.14 mmol) and acetic anhydride (0.30 mL, 2.57 mmol) in dichloromethane (5 mL) at room temperature. Triethylamine (0.35 mL, 4.28 mmol) was then added dropwise to the stirred solution. After 12 hours, the mixture was added with dichloromethane (15 mL) and was then extracted with water (2 × 20 mL). The organic layer was separated and dried over anhydrous $MgSO_4$ and evaporated under reduced pressure to obtain **Q1** as yellow light oil 550 mg (quantitative yield). ^{1}H NMR: (400 MHz, $CDCl_3$) δ 8.90 (d, J = 4.0 Hz, 1H), 8.10 (d, J = 8.3 Hz, 1H), 7.47 – 7.31 (m, 3H), 7.06 (d, J = 7.5 Hz, 1H), 4.36 (t, J = 5.0 Hz, 2H), 4.22 (t, J = 5.0 Hz, 2H), 4.03 (t, J = 5.0 Hz, 2H), 3.79 (t, J = 5.0 Hz, 2H), 2.03 (s, 3H); ^{13}C NMR: (101 MHz, $CDCl_3$) δ 170.85, 154.16, 149.06, 139.89, 136.32, 129.52, 126.98, 121.85, 119.98, 109.19, 69.45, 68.32, 63.58, 29.81, 20.75; MALDI-TOF m/z calculated for $C_{15}H_{17}NO_4$ [M]$^+$ 275.116, found 275.082.

2.3.2 Synthesis of **Q2**

- Synthesis of compound **2**
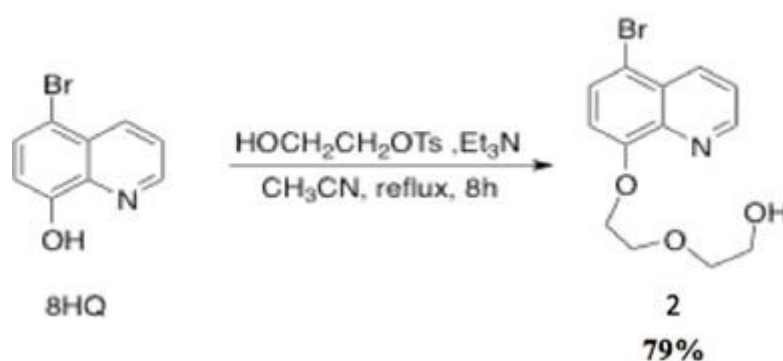
5-bromoquinolin-8-ol (300 mg, 1.33 mmol) and potassium carbonate (1,659 mg, 4 mmol) was stirred to dissolve in acetonitrile (5 mL). Dietyleneglycol monotorsylate (346 mg, 1.33 mmol) was added dropwise to this stirred solution. After reflux within 8 hours of stirring, the mixture was removed under reduced pressure. The yellow solid residue was dissolved in dichloromethane (20 mL) and then extracted with water (2 × 20 mL). The organic layer was dried over anhydrous $MgSO_4$ and the solvent was removed under reduced pressure. The obtained crude product was further purified by silica gel column chromatography using dichloromethane/ethyl acetate (7:3 v/v) mixture as the eluent to afford **2** (328 mg, 79% yield). ^{1}H NMR (400 MHz, CDCl$_3$) δ 8.92 − 8.82 (m, J = 4.2, 1.5 Hz, 1H), 8.45 (d, J = 8.6, 1.5 Hz, 1H), 7.66 (d, J = 8.4 Hz, 1H), 7.49 (dt, J = 21.2, 10.6 Hz, 1H), 6.90 (d, J = 8.4 Hz, 1H), 4.35 − 4.22 (m, 2H), 4.06 (dd, J = 15.6, 10.8 Hz, 2H), 3.86 (s, 1H), 3.80 (t, J = 5.4 Hz, 2H), 3.75 − 3.66 (m, 2H).

Synthesis of compound **Q2**
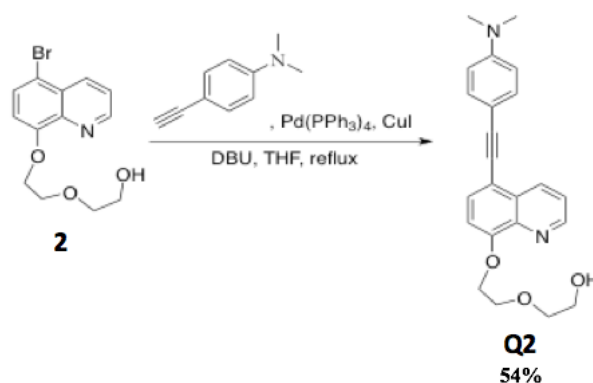
The solution of compound **2** (100 mg, 0.32 mmol) in THF (5 mL) and 1,8-diazabicyclo [5.4.0] undec-7-ene (0.1 mL) was bubbled thoroughly with nitrogen gas. Pd(PPh$_3$)$_4$ (3.7 mg, 1 mol%), CuI (0.6 mg, 1 mol%) and PPh$_3$ (0.4 mg, 0.1 mol%) were added to this solution and stirred for 10 min. Then, 4-ethynyl-*N,N*-dimethylaniline (70 mg, 0.48 mmol) was added dropwise to this mixture. The reaction mixture was heated to 80 °C while stirring. After 8 hours, water (20 mL) was added, and then extracted with ethyl acetate (2 × 20 mL). The organic layer was separated and dried over anhydrous MgSO$_4$ and the solvent was removed under reduced pressure. The obtained crude product was further purified by silica gel column chromato-graphy using dichloromethane /methanol mixture as the eluent to afford **Q2** (65 mg, 54 % yield). ^{1}H NMR (400 MHz, CD$_3$OD) δ 8.86 (d, 1H), 8.76 (d, *J* = 8.5, 1.5 Hz, 1H), 7.75 − 7.61 (m, 2H), 7.44 (d, *J* = 8.8 Hz, 2H), 7.20 (d, *J* = 18.1, 8.4 Hz, 1H), 6.76 (d, *J* = 8.8 Hz, 2H), 4.60 (s, 1H), 4.40 (t, 2H), 4.03 (t, 2H), 3.71 (dd, *J* = 6.8, 2.7 Hz, 4H), 3.00 (s, 6H). ^{13}C NMR (101 MHz, MeOD) δ 155.49 (s), 152.01 (s), 150.22 (s), 140.71 (s), 136.57 (s), 133.60 (s), 131.86 (s), 130.80 (s), 123.52 (s), 115.34 − 114.89 (m), 113.22 (s), 111.23 (s), 110.41 (s), 96.10 (s), 84.60 (s), 73.87 (s), 70.29 (s), 69.74 (s), 62.20 (s), 40.42 (s). MALDI-TOF m/z calculated for C$_{15}$H$_{17}$NO$_4$ [M]$^+$ 376.179, found 375.479.

2.3.3 Synthesis of **Q3**

- Synthesis of **Q3**
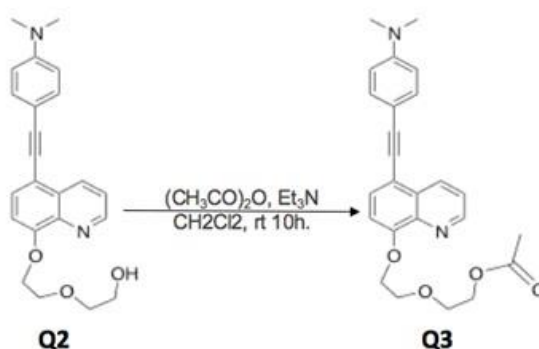
The acetylation of **Q2** (250 mg, 0.67 mmol) was conducted in the same manner with the acetylation of **1** described above to obtain yellow light oil of **Q3** 280 mg (quantitative yield). ^{1}H NMR: (400 MHz, CDCl$_3$) δ 8.99 (s, 1H), 8.75 (d, J = 7.2 Hz, 1H), 7.69 (m, 1H), 7.58 – 7.43 (m, 3H), 7.10 (d, J = 7.7 Hz, 1H), 6.70 (d, J = 8.6 Hz, 2H), 4.45 (t, J = 3.2 Hz, 2H), 4.26 (t, J = 3.2 Hz, 2H), 4.09 (t, J = 4.0 Hz, 2H), 3.83 (t, J = 4.0 Hz, 2H), 3.01 (s, 6H), 2.06 (s, 3H); ^{13}C NMR: (101 MHz, CDCl$_3$) δ 171.06, 153.73, 150.17, 149.63, 139.22, 135.86, 132.71, 130.77, 129.73, 123.05, 114.73, 111.69, 110.18, 95.15, 83.98, 66.99, 62.59, 53.09, 43.46, 40.20, 29.51, 20.93; MALDI-TOF m/z calculated for C$_{26}$H$_{29}$N$_2$O$_4$ [M]$^+$ 418.189, found 418.503.

2.4 Photophysical property study

2.4.1 UV-Visible spectroscopy

The stock solutions of **8HQ, Q1, Q2 and Q3** (0.01 mM) in acetonitrile were prepared. The absorption spectra of all fluorophores were recorded from 200 nm to 500 nm at ambient temperature.

2.4.1.1. Molar Absorption Coefficients (ε)

Molar Absorption Coefficients (ε) of all fluorophores were estimated from UV absorption spectra of analytical samples in CH_3CN for the sensors base on calix[4]arene derivatives and in DMSO for the hydrazide sensors at various concentrations. The intensities at absorption maximum wavelength (λ_{max}) of each compound were plotted against the concentrations. Each plot should be a straight line goes through origin. Molar Absorption Coefficients (ε) can be obtained from plotting of maximum absorption (A) vs concentration (C) represented into the following equation:

$$A = \varepsilon bC$$

*b is the cell path length.

2.4.2 Fluorescence spectroscopy

The stock solutions of **8HQ, Q1, Q2** and **Q3** were dilute to 1 μM in acetonitrile and methanol. The emission spectra of **8HQ** and **Q1** were recorded from 330 nm to 700 nm while **Q2** and **Q3** were recorded 390 nm to 700 nm at ambient temperature usiang an excitation wavelength at 310 to 370 nm.

2.4.3 Fluorophore quantum yields

The fluorescence quantum yields of **Q3** were performed in 30/70 %v/v CH_3OH/HEPES (pH 7.4, 1 mM). Each sample used quinine sulphate (Φ_{ST} = 0.54: λ_{ex} 336 nm) in 0.5 M H_2SO_4 or fluorescein (Φ_{ST} = 0.95: λ_{ex} 496 nm) in 0.1 M NaOH as a reference [44]. The UV-Vis absorption spectra of five analytical samples and five reference samples at varied concentrations were recorded. The maximum absorbance of all samples should never exceed 0.1. The fluorescence emission spectra of the same solution using appropriate excitation wavelengths selected were recorded based on the absorption maximum wavelength (λ_{max}) of each compound. Graphs of integrated fluorescence intensities were plotted against the absorbance at the respective

excitation wavelengths. Each plot should be a straight line with 0 interception and gradient *m*. In addition, the fluorescence quantum yield (Φ_x) was obtained from plotting of integrated fluorescence intensity *vs* absorbance represented into the following equation:

$$\Phi_X = \Phi_{ST}\left(\frac{Grad_X}{Grad_{ST}}\right)\left(\frac{\eta_X^2}{\eta_{ST}^2}\right)$$

The subscripts Φ_{ST} denote the fluorescence quantum yield of a standard reference Φ_X is the fluorescence quantum yield of sample and η is the refractive index of the solvent.

2.5 Fluorescent sensor study

2.5.1 Selectivity study

All stock metal ions such as Na^+, Mg^{2+}, Al^{3+}, K^+, Ca^{2+}, Fe^{2+}, Co^{2+}, Ni^{2+}, Cu^{2+}, Zn^{2+}, Ag^+, Hg^{2+}, Cd^{2+} and Pb^{2+} were prepared in Milli-Q water and adjusted to 1mM. The stock solution of **8HQ**, **Q1**-**Q3** (0.1 mM) in acetonitrile and methanol 100 was added in a 1 mL quartz cuvette. 100 μL of various metal ions (100 μM) was separately added into the sensor solutions at the ratio 1:10 of fluorophore to analyte. The final volumes were adjusted to 1 mL by adding HEPES buffer (pH7.4, 1mM). The emission spectra of **8HQ** and **Q1** sensors were recorded from 330 nm to 700 nm at ambient temperature using an excitation wavelength at 300-315 nm. The emission spectra of **Q2** and **Q3** were recorded from 390 to 700 nm at ambient temperature using an excitation wavelength at 370 nm.

2.5.2 Fluorescence titration

The stock solution of the sensing compound in MeOH (0.1 mM, 10 μL) was diluted with HEPES buffer pH 7.4 (1 mM, 900 μL) in a 1 mL quartz cuvette. Designated volumes (0-100 μL) of the Hg^{2+} stock solution (10 mM) in the HEPES buffer was added into the sensor solution. The final volumes were adjusted to 1 mL by adding the

solution of HEPES buffer. The final concentration of each fluorophore is 10 μM in 30/70 CH$_3$OH/HEPES aqueous solution. The spectra were recorded using λ_{ex} = 370 nm.

2.5.3 Interference study

All stock metal ions such as Na$^+$, Mg^{2+}, Al^{3+}, K$^+$, Ca^{2+}, Fe^{2+}, Co^{2+}, Ni^{2+}, Cu^{2+}, Zn^{2+}, Ag$^+$, Hg^{2+}, Cd^{2+} and Pb^{2+} were prepared in Milli-Q water and adjusted to 1mM. The stock solution of **Q3** (0.1 mM) in methanol 100 was added in a 1 mL quartz cuvette. 100 μL of analyte (100 μM) was separately added into the sensor solutions. Then, 100 μL of various metal ions except analyte was added in the solution at the ratio was 1:10:10 of sensor to analyte to interference. The final volumes were adjusted to 1 mL by adding HEPES buffer (pH 7.4 1mM). The emission spectra of **8HQ** and **Q1** sensors were recorded from 330 nm to 700 nm at ambient temperature using an excitation wavelength at 300-315 nm. The emission spectra of **Q2** and **Q3** were recorded from 390 to 700 nm at ambient temperature using an excitation wavelength at 370 nm.

2.5.4 Limit of detection

In fluorescent sensing, limit of detection (LOD) is the lowest concentration of analyte in a sample that is required to produce a signal greater than three times the standard deviation of the blank sample. But the value is not necessarily quantitated as an exact value.

2.5.3.1 Limit of detection for turn-off sensing

For turn-off sensing, the limit of detection can be calculated according to the equation) (5) and the Stern-Volmer equation (4). *SD* is the standard deviation of the response deriving from intensity of a fluorophore in the absence of an analyte (n = 9). I_0 is the fluorescent intensity of the blank sample (sensor in the absence of quencher), I is the observed fluorescent intensity with [Q] present. The Stern-Volmer constant K$_{sv}$ is determined from the slope of the Stern-Volmer plot as shown example in Figure 2.1.

$$LOD = [I_0/(I_0-3SD)-1]/K_{sv} \qquad (5)$$

2.5.3.2 Limit of detection for turn-on sensing

For turn-on sensing, the limit of detection can be calculated according to the equation (6):

$$LOD = [(I_0+3SD)/I_0-Intercept]/K \qquad (6)$$

The variables were similar to those in turn-on sensing. Except K is the slope of the straight line of the plot of I/I_0 against the concentration of an analyte [A]. Example of the calibration curve is shown in Figure 2.17.
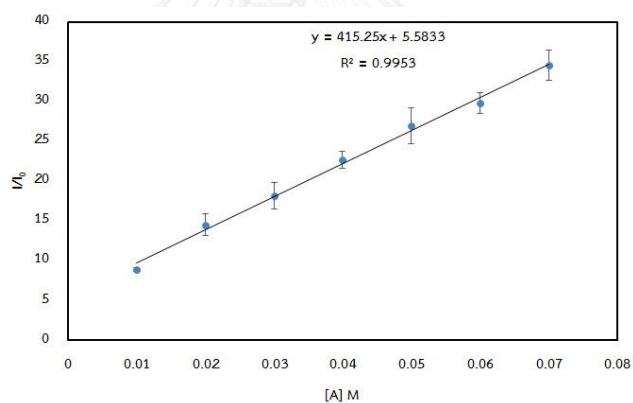
Figure 2.1 The calibration curve for turn-on sensing

CHAPTER III

RESULTS AND DISCUSSION

3.1 Synthesis and characterization of **Q1**, **Q2** and **Q3**

The 8-hydroxyquinoline derivatives **Q1**, **Q2** and **Q3** were synthezied from 8-hydroxyquinoline and 5-bromo-8-hydroxyquinoline as shown in Figure 3.1. First, compound **1** was prepared in 89% yield from 8-hydroxyquinoline and (hydroxymethoxy)methyl 4-methylbenzyene sulfonate in basic catalysed. Then, the acetylation of **1** by using acetic anhydride gave **Q1** in quantitative yield. Following the same procedure that was described above for compound **1** but 5-bromoquinolin-8-ol (was used instead of 8-hydroxyquinoline gave compound **2** in 79% yield. The key step was Sonogashira coupling reaction between **2** and 4-ethynyl *N,N*-dimethylaniline to give compound **Q2**. Then, the acetylation reaction of **Q2** gave **Q3** in quantitative yield.
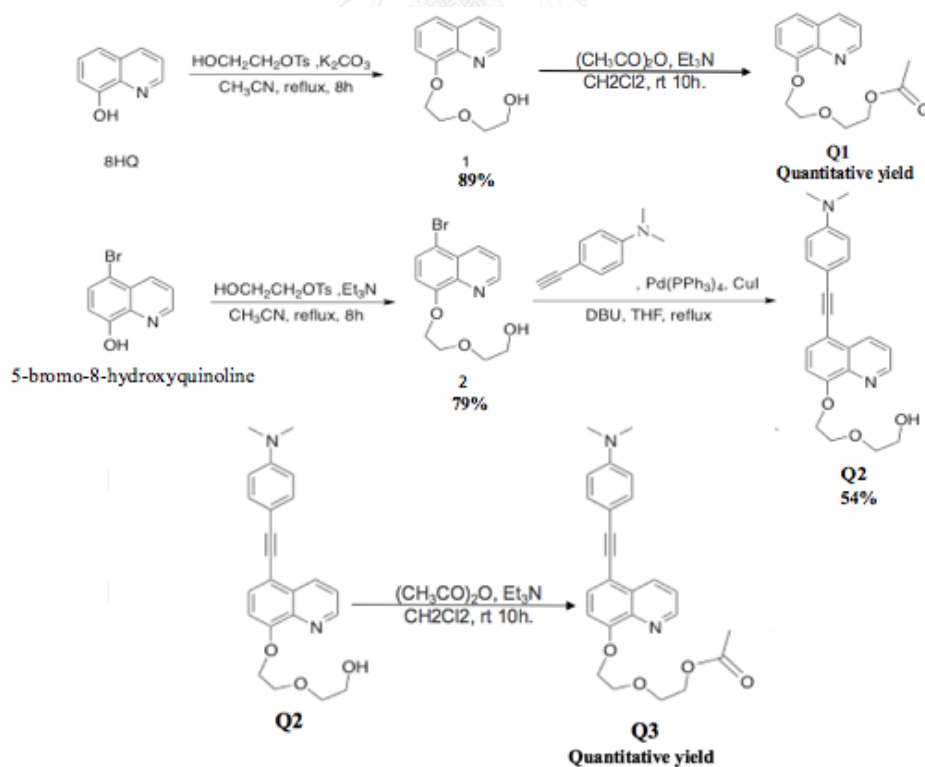
Figure 3.1 Synthesis scheme of **Q1**, **Q2** *and* **Q3**

The ^{1}H NMR spectra of compound **1** and **Q1** in CDCl$_3$ are shown in Figure 3.2. All the peaks can be assigned to all the protons in each corresponding structure. The methoxy protons on diethylene glycol chain appeared as four triplet peaks around 3.5 – 4.5 ppm that are characteristic peak for the completed modification. After acetylation of **1**, the singlet peak of -OH proton at 4.25 ppm was disappeared while a new singlet proton peak of the acetyl protons (CH$_3$CO-) show at 2 ppm.
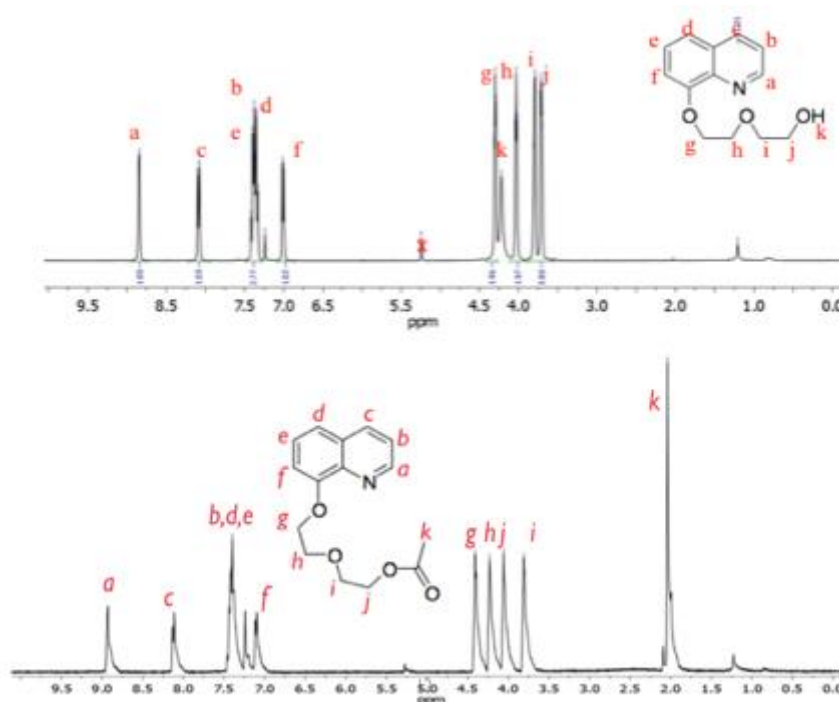
*Figure 3.2 ^{1}H NMR spectra of compounds **1** (top) and **Q1** (bottom)*

The ^{1}H NMR spectra of compound **2** in CDCl$_3$ and **Q2** in CD$_3$OD are shown in Figure 3.3. All the peaks can be assigned to all the protons in each corresponding structure. Two new doublet peaks at 6.8 ppm and 7.4 ppm of **Q2** were characteristic peaks of symmetrical aromatic protons on dimethylaniline. The hydroxyl proton (-OH) of **Q2** was observed in a protic solvent that conform an intramolecular H-bonding between -OH and N on quinoline ring.
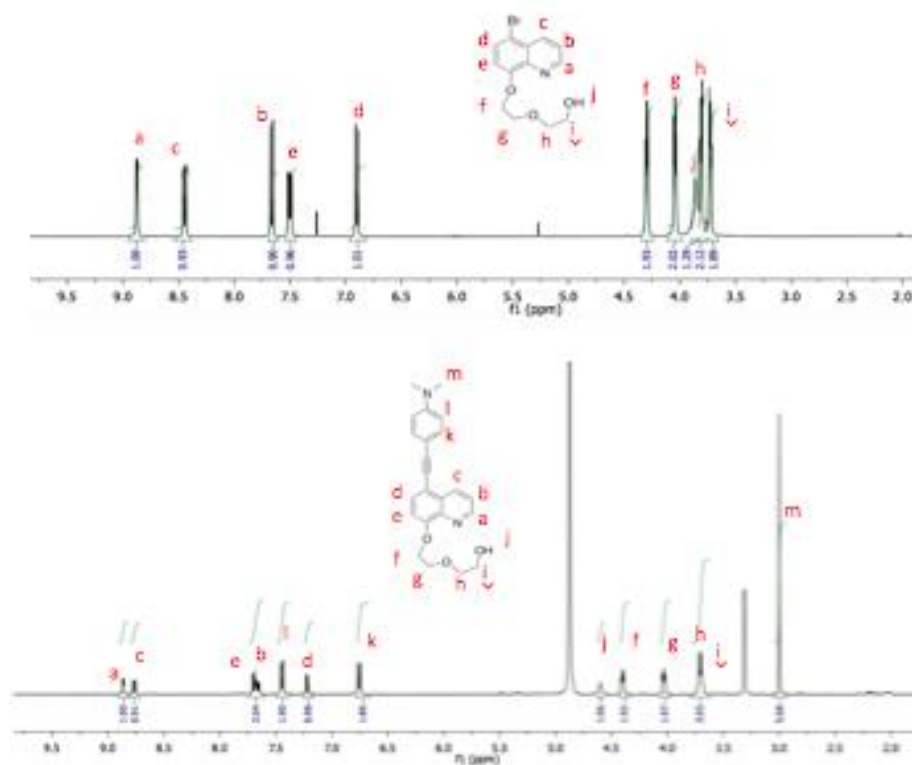
*Figure 3.3 ¹H NMR spectra of compounds **2** (top) and **Q2** (bottom)*

The ¹H NMR spectrum of **Q3** in CDCl₃ are shown in Figure 3.4. After acetylation, **Q3** was confirmed by appearance of the acetyl proton peak around 2 ppm.
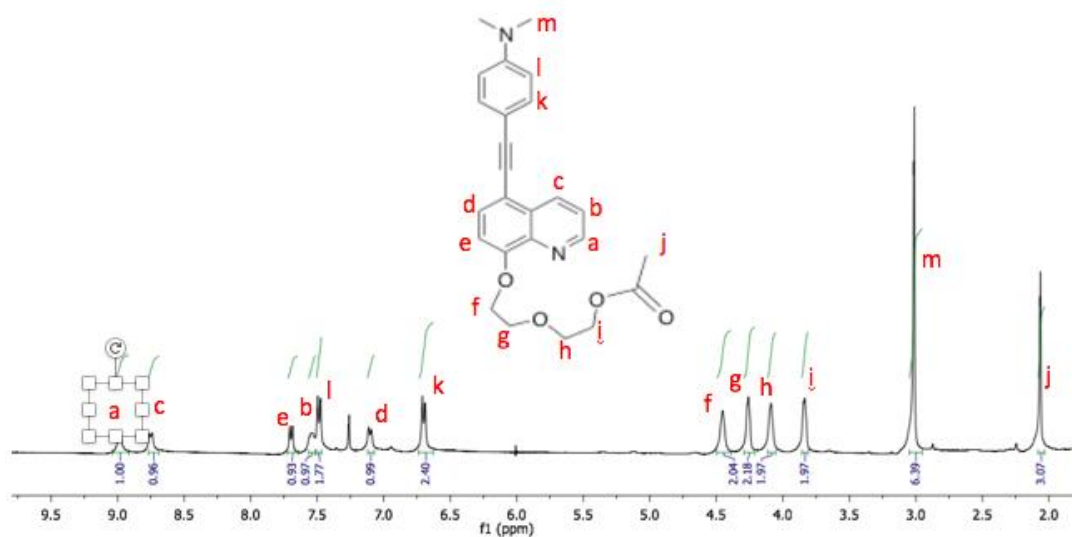
Figure 3.4 ^{1}H NMR spectra of compounds Q3

3.2 Photophysical properties of **8HQ, Q1, Q2** and **Q3**
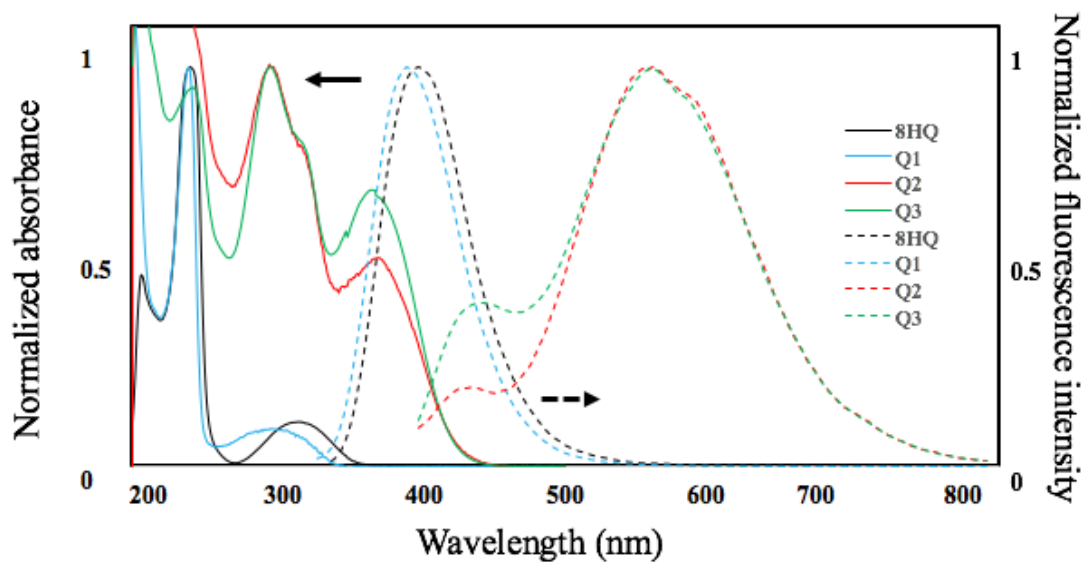
Figure 3.5 Normalized absorption and emission spectra of 8-hydroxyquinoline

derivatives (10 μM) in CH$_3$CN solution

The absorption and emission spectra of **8HQ** and three derivatives were determined in CH₃CN solution (Figure 3.5). Every compound showed absorption peak around 290-313 nm. For **8HQ** and **Q1**, the absorption spectra were similar and the maximum absorption peak was observed at 240 nm. For **Q2** and **Q3**, another absorption peak was observed at 366 nm and 370 nm, respectively, which correspond to the extended **π**-conjugated system. For more understanding, the calculated absorption peak of **Q1** and **Q3** was determined by Density Functional Theory (DFT) with the B3LYP/6-311G++ as a basis set (Table 3.1). The maximum absorption peak at 240 nm in **Q1** was corresponding to electronic transition from HOMO to LUMO+1 while the longer absorption peak at 291 nm was transition from HOMO to LUMO. To Compared with **Q3**, the calculation bang gaps in HOMO-LUMO+1 and HOMO-LUMO were decreased and shifted absorption peak at 295 nm and 366 nm, respectively, due to longer **π**-conjugation system in **Q3** molecule. The fluorescence spectrum of **Q1** was similar to that of **8HQ** which contained an emission maximum around 400 nm. For **Q2** and **Q3**, the emission bands were observed at 560 nm and the shoulder at 450 nm. Under the black light, the solutions of **Q2** and **Q3** showed significantly stronger emission than **8HQ** at the same concentration (photographs in Table 1) that may be due to the lack of the excited state intramolecular proton transfer (ESIPT) between the O and N atoms.

Table 3.1 Photophysical properties of 8-hydroyquinoline derivatives

Compound	Adsorption				Emission	
	$\lambda_{abs}{}^a$ (nm)	ε (cm^{-1} M^{-1})	$\lambda_{cal}{}^b$ (nm)	Corresponding orbit [b]	$\lambda_{em}{}^a$ (nm)	Fluorescence appearance
HQ	240	6,700	-	-	400	
	313	2,700	-	-		
Q1	240	39,100	237	HOMO -> LUMO+1	390	
	291	3,600	284	HOMO -> LUMO		
Q2	297	19,300	-	-	560	
	370	11,200	-	-		
Q3	295	21,700	288	HOMO -> LUMO+1	560	
	366	14,700	370	HOMO -> LUMO		

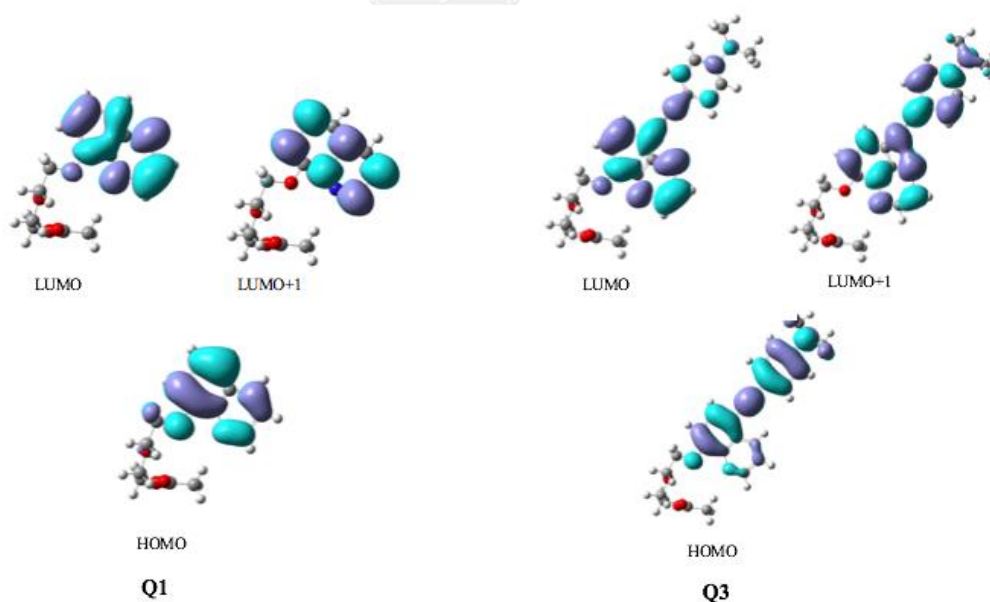[a] in acetonitrile solution [b] calculated by TD-DFT B3LYP/6-311G++

Figure 3.6 Optimized frontier molecular orbital of **Q1** and **Q3** by DFT with the

B3LYP/6-311G++ basis set

3.3 Effects of solvents on absorption and emission

The investigation of intramolecular charge transfer (ICT) process, the absorption and emission spectra of **Q3** (10μM) were determined in various solvents (Figure 3.7-3.8). The absorption peaks of **Q3** were slightly change but the emission was significantly red-shifted from 430 to 570 nm when raising the polarity of solvents that called bathochromic shift. The bathochromic shift may be corresponding to an excited intramolecular charge transfer (ICT) process from electron push-pull in the π-conjugated system. To illustrated the ICT process, the frontier molecular orbitals were optimized by DFT with the B3LYP/6-311G++ as basis set (Figure 3.6). The HOMO and LUMO in **Q3** showed the electron delocalization from the dimethylamino group to the quinoline rings which induced the intramolecular charge transfer in excited state. Moreover, **Q3** showed strongly fluorescence in aprotic solvents which observed by naked-eye under blacklight (inset in Figure 3.8). Interestingly, the polar protic solvent, CH$_3$OH, **Q3** was quenched the fluorescence signal due to the hydrogen bonding formation of the lone pair on the amino moiety [45]. Therefore, the polar aprotic solvent was suitable for turn-off sensing while the polar protic solvent was good for turn-on sensing.
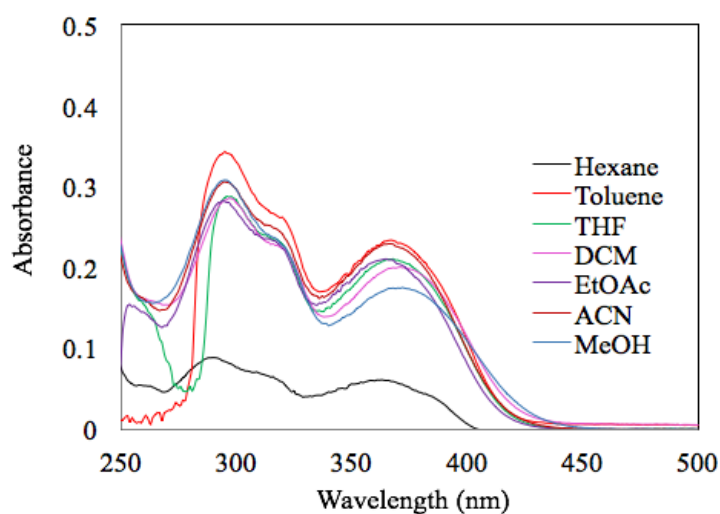

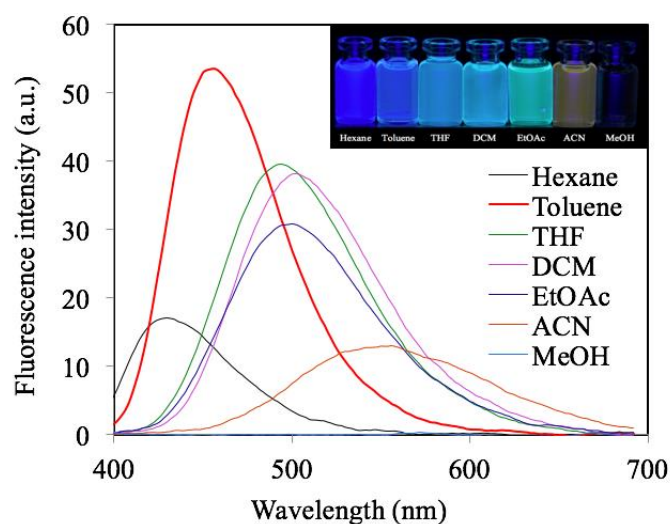*Figure 3.7 Absorption spectra of **Q3** (10 μM) in various solvents*

Figure 3.8 Emission spectra of Q3 in various solvents; inset photographs under the blacklight (365 nm)

3.4 Metal ions selectivity study

The metal ions sensing properties of **8HQ**, **Q1**, **Q2** and **Q3** were studied in acetonitrile-water and methanol-water solution. In acetonitrile-water condition, the fluorescence response ratios (I/I_0) of the **8HQ** and derivatives (10 μM) were tested with various metal ions (100 μM) in 90:10 (v/v) CH_3CN/HEPES solution (1 mM, pH 7.4) (Figure 3.9). **8HQ** has no selectively with any metal ions in the acetonitrile-water solution. Surprisingly, **Q1** gave intensive fluorescence enhancement at 490 nm with Al^{3+}, Cr^{3+} and Fe^{3+}. For other metal ions such as Na^+, Mg^{2+}, K^+, Ca^{2+}, Fe^{2+}, Co^{2+}, Ni^{2+}, Cu^{2+}, Zn^{2+}, Ag^+, Cd^{2+}, Hg^{2+} and Pb^{2+} gave no significant fluorescence change. Moreover, **Q2** and **Q3** were slightly quenched the fluorescence response by Al^{3+}, Cr^{3+} and Fe^{3+}. In methanol-water condition, the fluorescence response ratios (I/I_0) of the synthesized compounds along with **8HQ** (10 μM) were tested with various metal ions (100 μM) in 30:70 (v/v) CH_3OH/HEPES solution (1 mM, pH 7.4). As shown in Figure 3.10, Surprisingly, **8HQ** gave fluorescence enhancement selectively to Al^{3+} in methanol solution. The Al^{3+} complex

of **8HQ** is a well-known green emissive material frequently studied in OLED. In contrast, **Q1** did not show any fluorescence responses to the metal ions in methanol solution. Serendipity, **Q3** showed a selective green fluorescence enhancement at 510 nm with Hg^{2+}. The other metal ions such as Na^+, Mg^{2+}, Al^{3+}, K^+, Ca^{2+}, Fe^{2+}, Co^{2+}, Ni^{2+}, Cu^{2+}, Zn^{2+}, Ag^+, Cd^{2+} and Pb^{2+} no obvious change was observed. According to the results above, the solvent effect was one of all factor for improved the sensing properties.
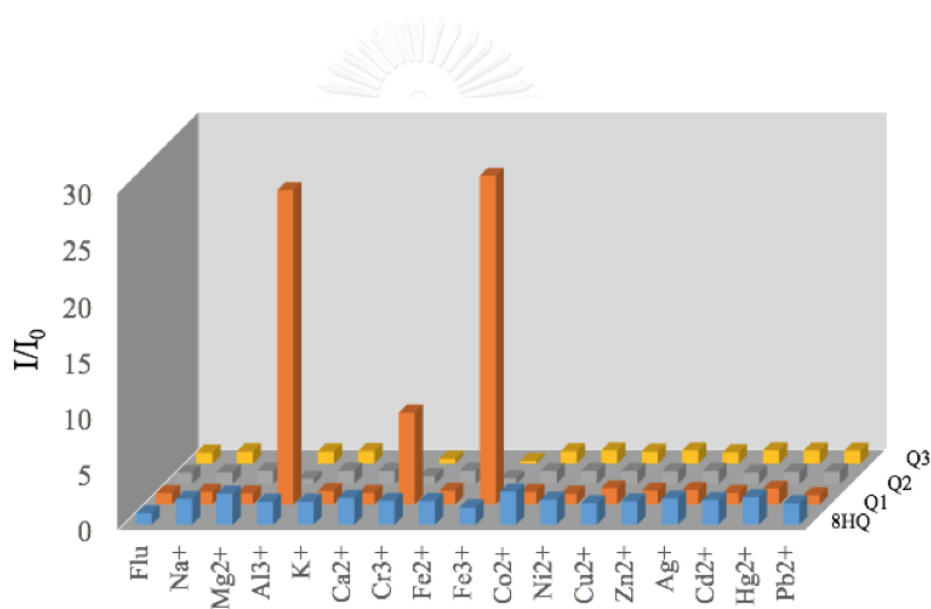

*Figure 3.9 fluorescence response ratios (I/I_0) of the **8HQ** and derivatives (10 μM) were tested with various metal ions (100 μM) in 90:10 (v/v) CH₃CN/HEPES solution (1 mM, pH 7.4)*
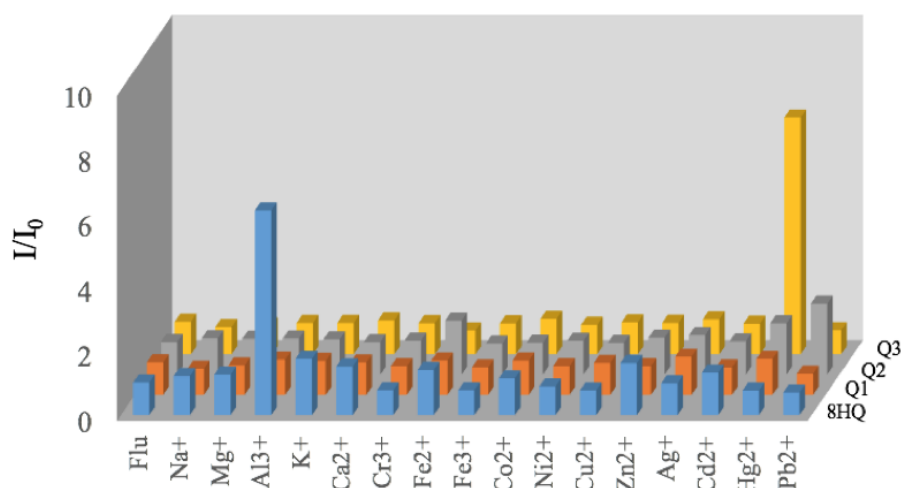
*Figure 3.10 fluorescence response ratios (I/I_0) of the **8HQ** and derivatives (10 **μ**M)
were tested with various metal ions (100 **μ**M) in 70:30 (v/v) CH₃OH/HEPES solution (1
mM, pH 7.4)*

3.5 Sensitivity of **Q3** and interference in Hg2+ detection

The fluorescence responses of **Q3** (10 **μ**M) to Hg^{2+} at varied concentrations are shown in Figure 4a. The emission band at 510 nm gradually increased upon the addition of Hg^{2+}. The plot of I/I_0 against $[Hg^{2+}]$ was gradually increased and became saturated after 100 equivalents of Hg^{2+} (Figure 3.11). The saturation of the fluorescence response at very high equivalent of Hg^{2+} suggested that the fluorescence enhancement of **Q3** by Hg^{2+} was a non-stoichiometric process. However, a linear response was observed in the low concentration range of 1-10 **μ**M (R^2 = 0.973). The detection limit of Hg^{2+} was 64 nM (or 13 ppb) as determined by 3σ/slope (S/N = 3 criteria). For the interference of other metal ions to the Hg^{2+} detection with **Q3**, competitive experiments were performed by measuring the fluorescence response of **Q3** to Hg^{2+} in the presence of the interfering metal ion tested. The fluorescence response to Hg^{2+} was slightly quenched by some interfering metal ions as shown Figure 3.13.

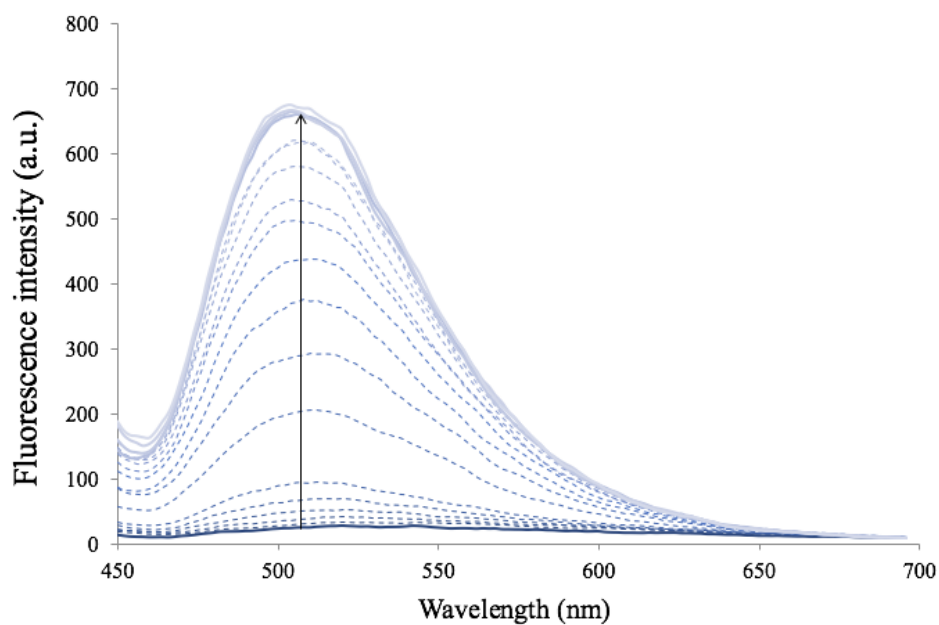Figure 3.11 Fluorescence intensity of 10 μM **Q3** (λex = 370 nm) upon addition of varied concentrations of Hg^{2+} in 30:70 (v/v) CH$_3$OH/HEPES solution (1 mM, pH 7.4)
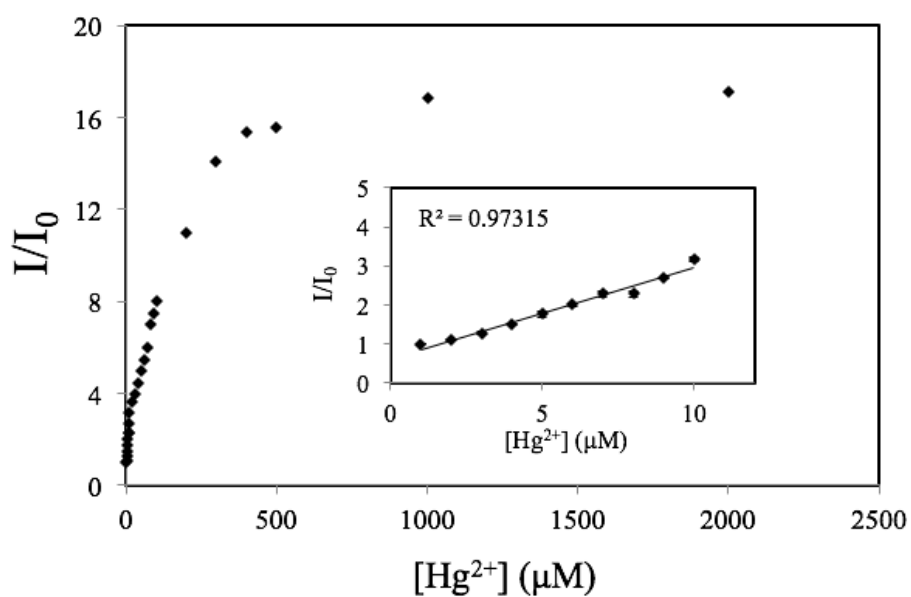
Figure 3.12 Plot of I/I$_0$ at 500 nm versus [Hg^{2+}]; inset shows linear range.
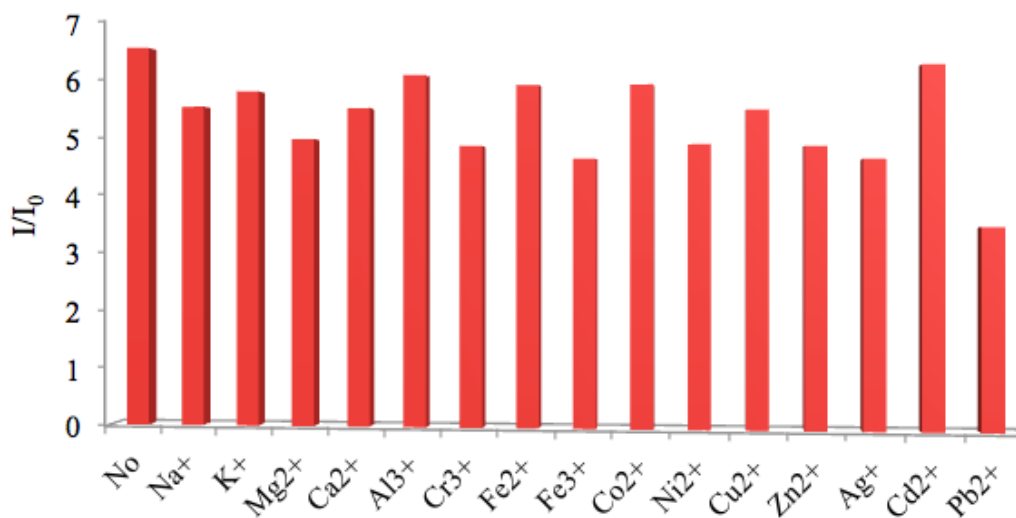
Figure 3.13 Competitive selectivity of Q3 (10 μM) toward Hg^{2+} ions (100 μM) in the

presence of other metal ions (100 μM) in 30:70 (v/v) CH$_3$OH/HEPES solution (1 mM,

pH 7.4)

3.6 Mechanism for fluorescence enhancement of Q3 by Hg^{2+}

The effect of solution media for Hg^{2+} detection with **Q3** was studied at various fractions mixed with methanol as shown in Figure 3.14. The maximum fluorescence response ratio (I/I$_0$) was observed at 70% water in methanol and this condition was suitable for Hg^{2+} detection. Since water is a non-solvent for **Q3**, the fluorescence enhancement may be due to the aggregation-induced emission (AIE) mechanism of **Q3** upon the binding with Hg^{2+}. The evidence for aggregation was observed by The Tyndall effect (Figure 3.14 right inset) and the solution gave strong green fluorescence under the black light (Figure 3.14 left inset).

*Figure 3.14 Fluorescence response (I/I$_0$) at 500 nm of **Q3** (10 μM, λ_{ex} 370 nm) to Hg^{2+} (10 equiv.) in methanol:water at various v/v ratios (HEPES solution 1 mM, pH 7.4); inset is a photograph of **Q3** at 30:70 ratio under black light in the absence and presence of Hg^{2+} (100 equiv.) and in the Tyndall experiment.*
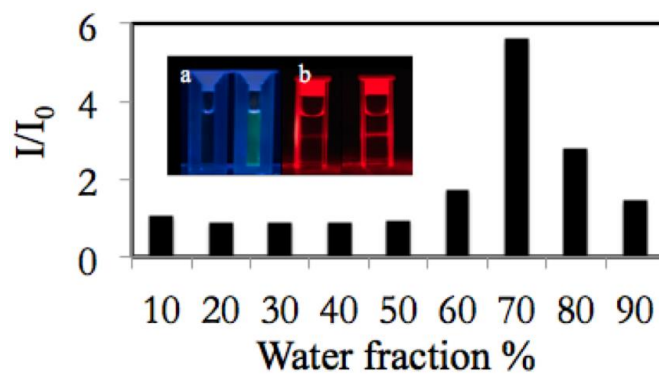
CHAPTER IV

CONCLUSION

In conclusion, the three new 8-hydroxyquinoline (**8HQ**) derivatives (**Q1**, **Q2** and **Q3**) have been successfully synthesized and characterized. The absorption spectra of Q1 was similar to 8HQ having two absorption maxima around 240 and 300 nm, while those of Q2 and Q3 showed two absorption peaks at longer wavelength around 300 and 370 nm. The emission maximum of Q2 and Q3 was also red-shifted, from 400 nm observed for 8HQ and Q1, to 560 nm. The metal ions sensing test in 90:10 v/v CH_3CN/HEPES solution (1 mM, pH 7.4) showed that the fluorescence of Q1 was selectively enhanced with trivalent metal ions such as Al^{3+}, Cr^{3+} and Fe^{3+}, while 8HQ, Q2 and Q3 gave low fluorescence response and were non-selective to metal ions. In 30:70 v/v CH_3OH/HEPES solution (1 mM, pH 7.4), 8HQ exhibited a well-known green fluorescence enhancement with Al^{3+} while Q3 showed interestingly strong green fluorescence (510 nm) enhancement selectively with Hg^{2+}. The linear fluorescence response range of Q3 was observed at 2-9 uM Hg^{2+} with the detection limit of 64 nM or 13 ppb. The Tyndall effect observed along with the increase of fluorescence intensity of Q3 upon the addition of Hg^{2+} suggests that the fluorescence enhancement of Q3 with Hg^{2+} was due to the aggregation induced emission (AIE).

For future works, the different effects of hydroxyl and acetyl group in **Q2** and Q3 on their fluorescence responses should be further investigated to verify the role of hydrogen bonding. The measurement of fluorescence life-time in H_2O and D_2O should provide information about the involvement of hydrogen bonding in ACQ of Q2 and AIE of Q3. The measurement of temperature dependence of the fluorescence intensity can also confirm the role of hydrogen bonding in ACQ of Q2 and AIE of Q3. The study of acetyl ester of Q1 is also interesting for completing of the series of these 8HQ derivatives.

REFERENCES

[1]   Gunnlaugsson, T., Ali, H., Glynn, M., Kruger, P., Hussey, G., Pfeffer, F., dos Santos, C., and Tierney, J. Fluorescent Photoinduced Electron Transfer (PET) Sensors for Anions; From Design to Potential Application. Journal of Fluorescence 15(3) (2005): 287-299.

[2]   Callan, J.F., de Silva, A.P., and Magri, D.C. Luminescent Sensors and Switches in the Early 21st century. Tetrahedron 61(36) (2005): 8551-8588.

[3]   de Silva, A.P., Gunaratne, H.Q., Gunnlaugsson, T., Huxley, A.J.M., McCoy, C.P., Radamacher, J.T. and Rice, T.E. Signaling Recognition Events with Fluorescent Sensors and Switches. Chemical Reviews 97(5) (1997): 1515-1566.

[4]   Martínez-Máñez, R. and Sancenón, F. Fluorogenic and Chromogenic Chemosensors and Reagents for Anions. Chemical Reviews 103(11) (2003): 4419-4476.

[5]   Valeur, B. and Leray, I. Design Principles of Fluorescent Molecular Sensors for Cation Recognition. Coordination Chemistry Reviews 205(1) (2000): 3-40.

[6]   Xu, Z., Yoon, J., and Spring, D.R. Fluorescent Chemosensors for Zn^{2+}. Chemical Society Reviews 39(6) (2010): 1996-2006.

[7]   Kim, J.S. and Quang, D.T. Calixarene-Derived Fluorescent Probes. Chemical Reviews 107(9) (2007): 3780-3799.

[8]   Sapsford, K.E., Berti, L., and Medintz, I.L. Materials for Fluorescence Resonance Energy Transfer Analysis: Beyond Traditional Donor–Acceptor Combinations. Angewandte Chemie International Edition 45(28) (2006): 4562-4589.

[9]   Carlson, H.J. and Campbell, R.E. Genetically Encoded FRET-Based Biosensors for Multiparameter Fluorescence Imaging. Current Opinion in Biotechnology 20(1) (2009): 19-27.

[10]   Wu, J., Liu, W., Ge, J., Zhang, H., and Wang, P. New Sensing Mechanisms for Design of Fluorescent Chemosensors Emerging in Recent Years. Chemical Society Reviews 40(7) (2011): 3483-3495.

[11]   Peng, X., Wu, Y., Fan, J., Tian, M., and Han, K. Colorimetric and Ratiometric Fluorescence Sensing of Fluoride: Tuning Selectivity in Proton Transfer. The Journal of Organic Chemistry 70(25) (2005): 10524-10531.

[12]   Wu, J.-S., Liu, W.-M., Zhuang, X.-Q., Wang, F., Wang, P.-F., Tao, S.-L., Zhang, X.-H., Wu, S.-K., Lee, S.-T. Fluorescence Turn On of Coumarin Derivatives by Metal Cations: A New Signaling Mechanism Based on C=N Isomerization. Organic Letters 9(1) (2007): 33-36.

[13]   Hong, Y., Lam, J.W.Y., and Tang, B.Z. Aggregation-Induced Emission: Phenomenon, Mechanism and Applications. Chemical Communications (29) (2009): 4332-4353.

[14]   Wang, M., Zhang, G., Zhang, D., Zhu, D., and Tang, B.Z. Fluorescent Bio/Chemosensors Based on Silole and Tetraphenylethene Luminogens with Aggregation-Induced Emission Feature. Journal of Materials Chemistry 20(10) (2010): 1858-1867.

[15]   Lodeiro, C. and Pina, F. Luminescent and Chromogenic Molecular Probes Based on Polyamines and Related Compounds. Coordination Chemistry Reviews 253(9–10) (2009): 1353-1383.

[16]   Introduction to Fluorescence. in Lakowicz, J. (ed.) Principles of Fluorescence Spectroscopy, pp. 1-26: Springer US, 2006.

[17]   Henary, M.M. and Fahrni, C.J. Excited State Intramolecular Proton Transfer and Metal Ion Complexation of 2-(2'-Hydroxyphenyl)benzazoles in Aqueous Solution. The Journal of Physical Chemistry A 106(21) (2002): 5210-5220.

[18]   Druzhinin, S.I., Mayer, P., Stalke, D., von Bülow, R., Noltemeyer, M., and Zachariasse, K.A. Intramolecular Charge Transfer with 1-tert-Butyl-6-cyano-1,2,3,4-tetrahydroquinoline (NTC6) and Other Aminobenzonitriles. A Comparison of Experimental Vapor Phase Spectra and Crystal Structures with Calculations. Journal of the American Chemical Society 132(22) (2010): 7730-7744.

[19]   Galievsky, V.A., Druzhinin, S.I., Demeter, A., Mayer, P., Kovalenko, S.A., Senyushkina, T.A. and Zachariasse, K.A. Ultrafast Intramolecular Charge Transfer with N-(4-Cyanophenyl)carbazole. Evidence for a LE Precursor and Dual LE + ICT Fluorescence. The Journal of Physical Chemistry A 114(48) (2010): 12622-12638.

[20]   Chung, S.-K., Tseng, Y.-R., Chen, C.-Y., and Sun, S.-S. A Selective Colorimetric Hg^{2+} Probe Featuring a Styryl Dithiaazacrown Containing Platinum(II) Terpyridine Complex through Modulation of the Relative Strength of ICT and MLCT Transitions. Inorganic Chemistry 50(7) (2011): 2711-2713.

[21]   Lakowicz, J.R. Principles of fluorescence spectroscopy. 3rd ed. New York: Springer, 2006.

[22]   Hong, Y., Lam, J.W.Y., and Tang, B.Z. Aggregation-induced Emission. Chemical Society Reviews 40(11) (2011): 5361-5388.

[23]   Bose-O'Reilly, S., Lettmeier, B., Matteucci Gothe, R., Beinhoff, C., Siebert, U., and Drasch, G. Mercury as a Serious Health Hazard for Children in Gold Mining Areas. Environmental Research 107(1) (2008): 89-97.

[24]   Clarkson, T.W. and Magos, L. The Toxicology of Mercury and Its Chemical Compounds. Critical Reviews in Toxicology 36(8) (2006): 609-662.

[25]   Fernandes, A., Lorena, B.F., Franck, M.P., Giulia, A.W., Paula, F.V., Maylla, R.S., Fiorim, J., Rossi de Batista, P., Fioresi, M., Rossoni, L., Stefanon, I., Alonso, M., Salaices, M., and Valentim Vassallo, D. Toxic Effects of Mercury on the Cardiovascular and Central Nervous Systems. Journal of Biomedicine and Biotechnology 2012 (2012): 11.

[26]   Dinda, D., Shaw, B.K., and Saha, S.K. Thymine Functionalized Graphene Oxide for Fluorescence "Turn-off-on" Sensing of Hg^{2+} and I^- in Aqueous Medium. ACS Applied Materials & Interfaces 7(27) (2015): 14743-14749.

[27]   Vaswani, K.G. and Keränen, M.D. Detection of Aqueous Mercuric Ion with a Structurally Simple 8-Hydroxyquinoline Derived ON-OFF Fluorosensor. Inorganic Chemistry 48(13) (2009): 5797-5800.

[28]   Shao, N., Pang, G.-X., Yan, C.-X., Shi, G.-F., and Cheng, Y. Reaction of β-Lactam Carbenes with 2-Pyridyl Isonitriles: A One-Pot Synthesis of 2-Carbonyl-3-(pyridylamino)imidazo[1,2-a]pyridines Useful as Fluorescent Probes for Mercury Ion. The Journal of Organic Chemistry 76(18) (2011): 7458-7465.

[29]   Wu, X., Niu, Q., Li, T., Cui, Y., and Zhang, S. A Highly Sensitive, Selective and Turn-Off Fluorescent Sensor Based on Phenylamine-Oligothiophene Derivative for Rapid Detection of Hg^{2+}. Journal of Luminescence 175 (2016): 182-186.

[30]   Vengaian, K.M., Britto, C.D., Sekar, K., Sivaraman, G., and Singaravadivel, S. Phenothiazine-diaminomalenonitrile Based Colorimetric and Fluorescence "Turn-off-on" Sensing of Hg2+ and S2–. Sensors and Actuators B: Chemical 235 (2016): 232-240.

[31]   He, J., et al. Carbon Dots-based Fluorescent Probe for "OFF-ON" Sensing of Hg(II) and I⁻. Biosensors and Bioelectronics 79 (2016): 531-535.

[32]   Zhang, R. and Chen, W. Nitrogen-doped Carbon Quantum Dots: Facile Synthesis and Application as a "Turn-Off" Fluorescent Probe for Detection of Hg2+ Ions. Biosensors and Bioelectronics 55 (2014): 83-90.

[33]   McClure, D.S. Spin-Orbit Interaction in Aromatic Molecules. The Journal of Chemical Physics 20(4) (1952): 682-686.

[34]   Bhalla, V., Tejpal, R., Kumar, M., and Sethi, A. Terphenyl Derivatives as "Turn On" Fluorescent Sensors for Mercury. Inorganic Chemistry 48(24) (2009): 11677-11684.

[35]   Ghosh, K. and Tarafdar, D. A new quinoline-based chemosensor in ratiometric sensing of Hg^{2+} ions. Supramolecular Chemistry 25(3) (2013): 127-132.

[36]   Wang, C., Cuicui, W,, Di, Z., Xiaoyan, H., Peigang, D., Zhenji, W., Yufen, Z. and Yong, Y. A Ratiometric Fluorescent Chemosensor for Hg^{2+} Based on FRET and Its Application in Living Cells. Sensors and Actuators B: Chemical 198 (2014): 33-40.

[37]   Sun, X., Shi, W., Ma, F., Hui, Y., Xu, L., Mi, H., Tian, Y. and Xie, Z.. Thymine-covalently decorated, AIEE-type Conjugated Polymer as Fluorescence Turn-On Probe for Aqueous Hg^{2+}. Sensors and Actuators B: Chemical 198 (2014): 395-401.

[38]   Soroka, K., Vithanage, R.S., Phillips, D.A., Walker, B., and Dasgupta, P.K. Fluorescence Properties of Metal Complexes of 8-hydroxyquinoline-5-sulfonic Acid and Chromatographic Applications. Analytical Chemistry 59(4) (1987): 629-636.

[39]   Montes, V.A., Pohl, R., Shinar, J., and Anzenbacher, P. Effective Manipulation of the Electronic Effects and Its Influence on the Emission of 5-Substituted Tris(8-quinolinolate) Aluminum(III) Complexes. Chemistry – A European Journal 12(17) (2006): 4523-4535.

[40]   Zhang, C.-L., Gong, S.-L., Luo, Z.-Y., Wu, X.-J., and Chen, Y.-Y. Synthesis, Characterization and Coordination Properties of a Novel Thiacalix[4]arene with Diagonal Quinolin-8-yloxy Pendants. Supramolecular Chemistry 18(6) (2006): 483-489.

[41]   Zhang, Y., Guo, X., Si, W., Jia, L., and Qian, X. Ratiometric and Water-Soluble Fluorescent Zinc Sensor of Carboxamidoquinoline with an Alkoxyethylamino Chain as Receptor. Organic Letters 10(3) (2008): 473-476.

[42]   Zhou, X., Li, P., Shi, Z., Tang, X., Chen, C., and Liu, W. A Highly Selective Fluorescent Sensor for Distinguishing Cadmium from Zinc Ions Based on a Quinoline Platform. Inorganic Chemistry 51(17) (2012): 9226-9231.

[43]   Pohl, R. and Anzenbacher, P. Emission Color Tuning in AlQ3 Complexes with Extended Conjugated Chromophores. Organic Letters 5(16) (2003): 2769-2772.

[44]   Brouwer Albert, M. Standards for Photoluminescence Quantum Yield Measurements in Solution (IUPAC Technical Report). in *Pure and Applied Chemistry*. 2011. 2213.

[45]   Chevreux, S., Allain, C., Wilbraham, L., Nakatani, K., Jacques, P., Ciofini I. and Lemercier G. Solvent Tuned Single Molecule Dual Emission in Protic Solvents: Effect of Polarity and H-bonding. Faraday Discussions 185(0) (2015): 285-297.
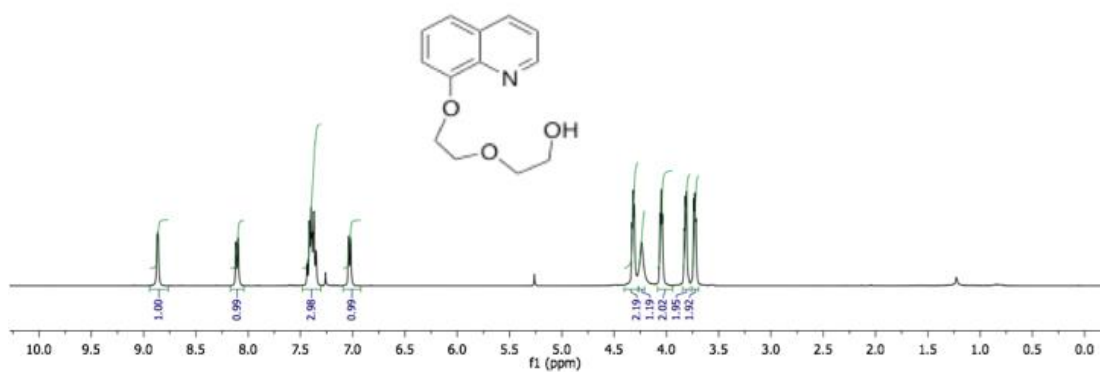
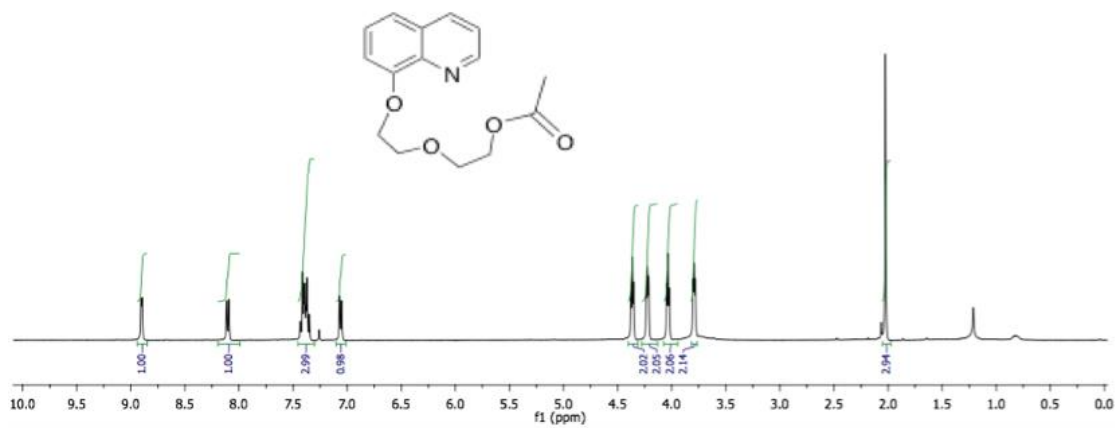APPENDIX

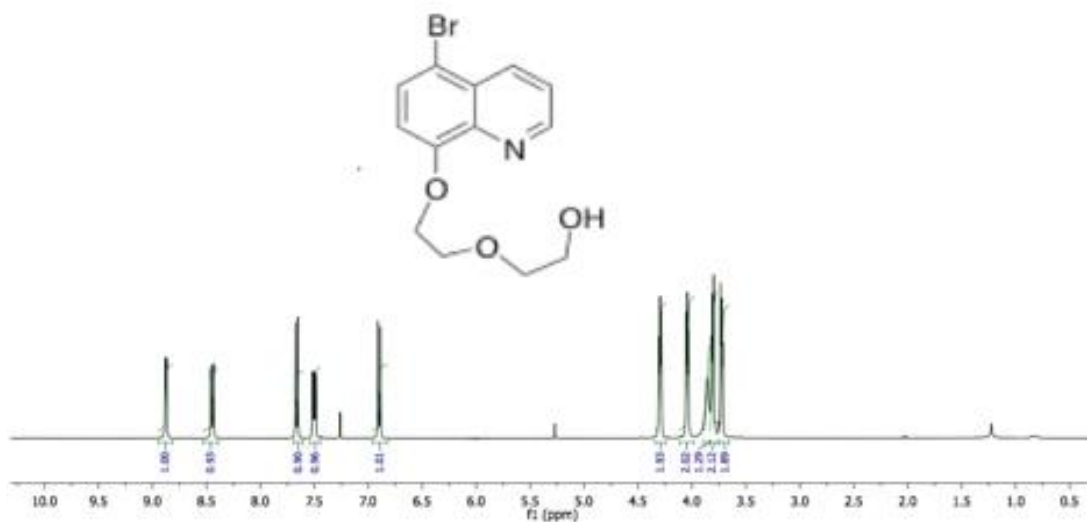Figure A.1 ^{1}H NMR of **1** in CDCl$_3$

Figure A.2 ^{1}H NMR of **Q1** in CDCl$_3$

Figure A.3 ^{13}C NMR of *Q1* in $CDCl_3$

Figure A.4 Mass spectrum of *Q1* obtained by MALDI-TOF

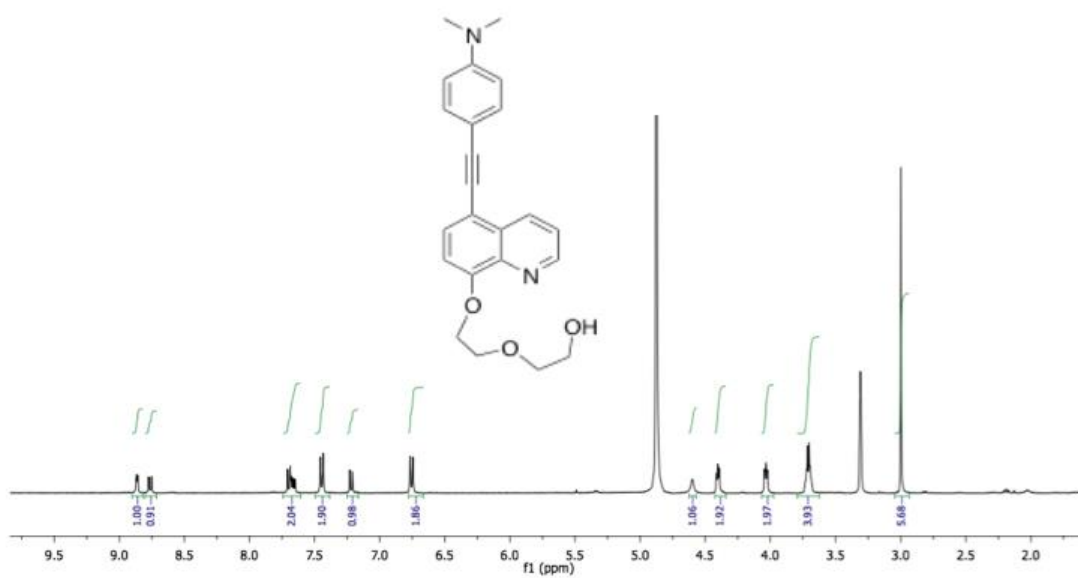Figure A.5 ^{1}H NMR of **2** in CDCl$_3$
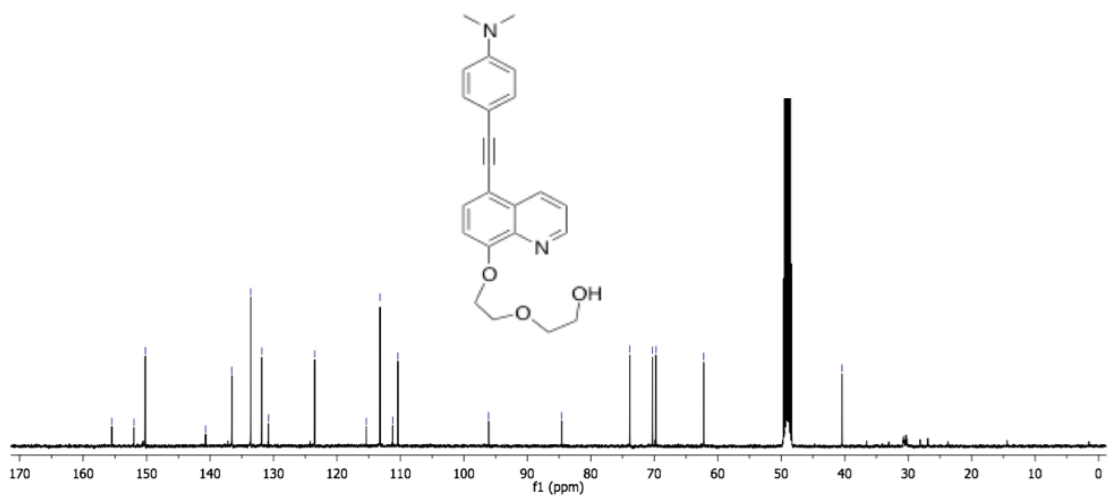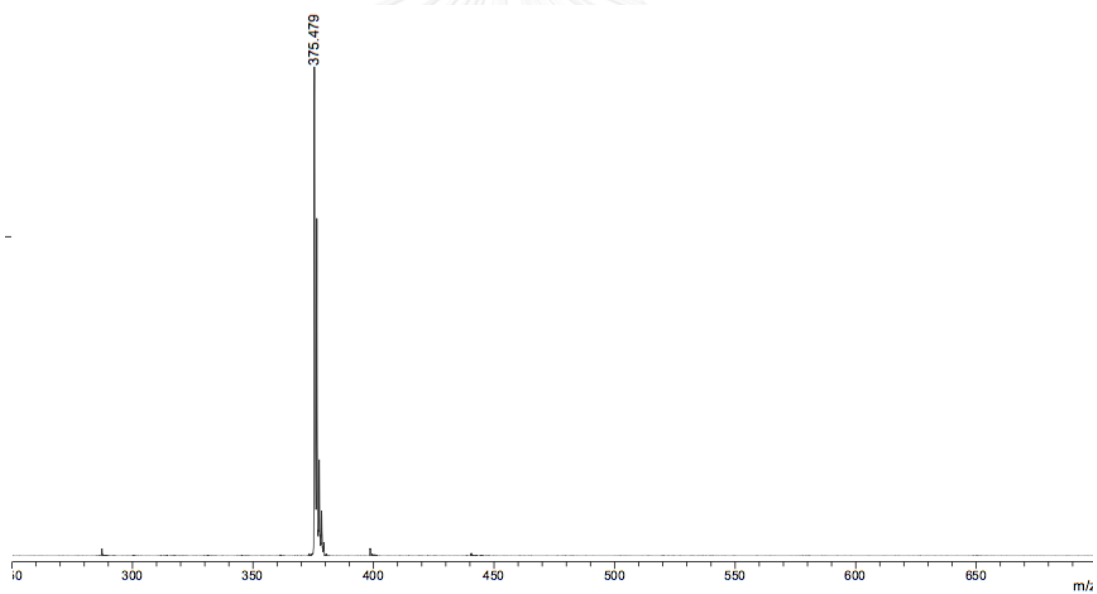

Figure A.6 ^{1}H NMR of **Q2** in CD$_3$OD

*Figure A.7 ^{13}C NMR of **Q2** in CD$_3$OD*

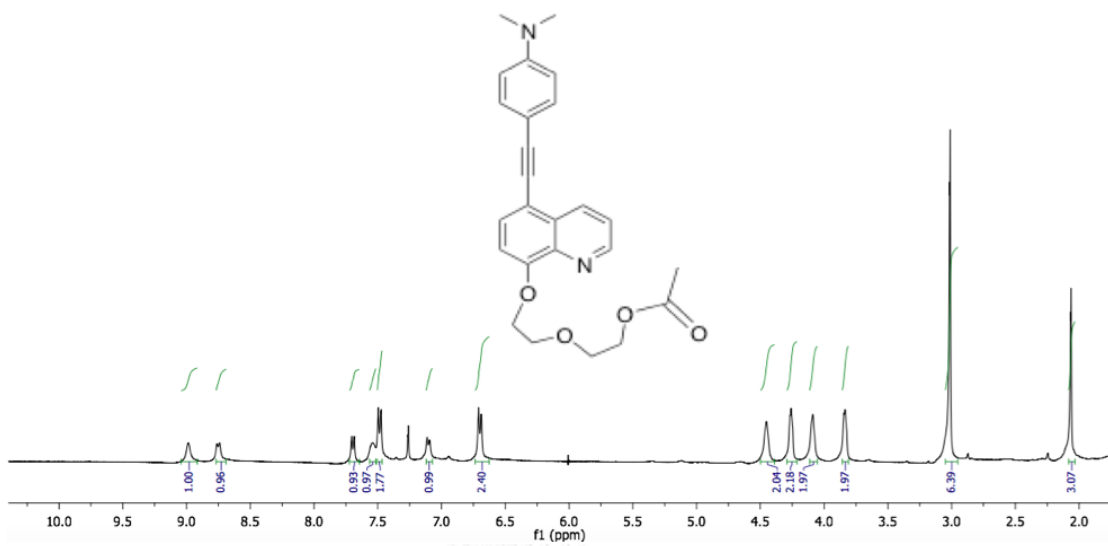

*Figure A.8 Mass spectrum of **Q2** obtained by MALDI-TOF*

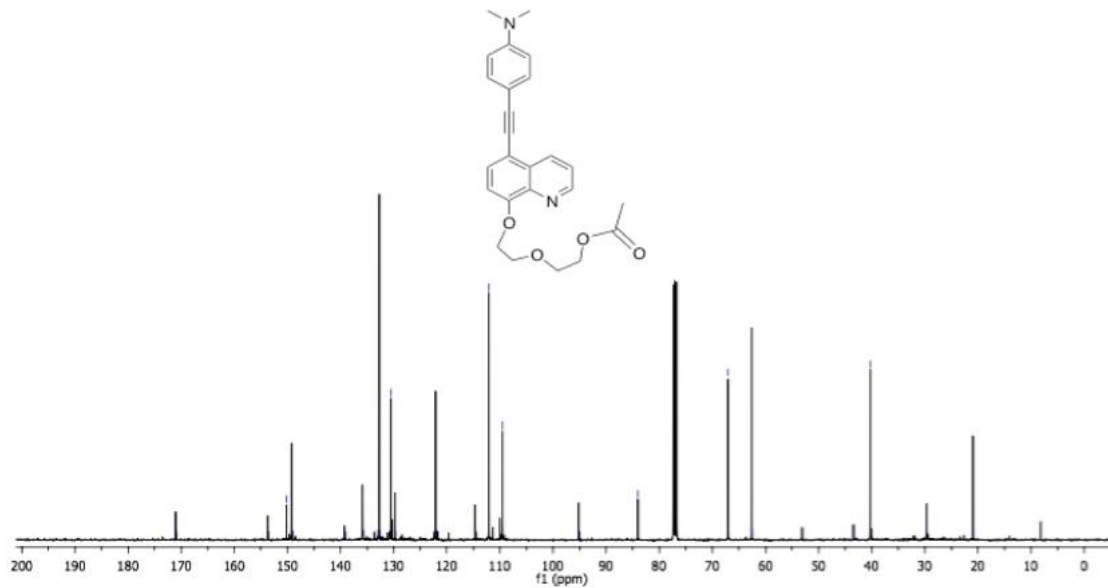Figure A.9 ^{1}H NMR of **Q3** in CDCl$_3$

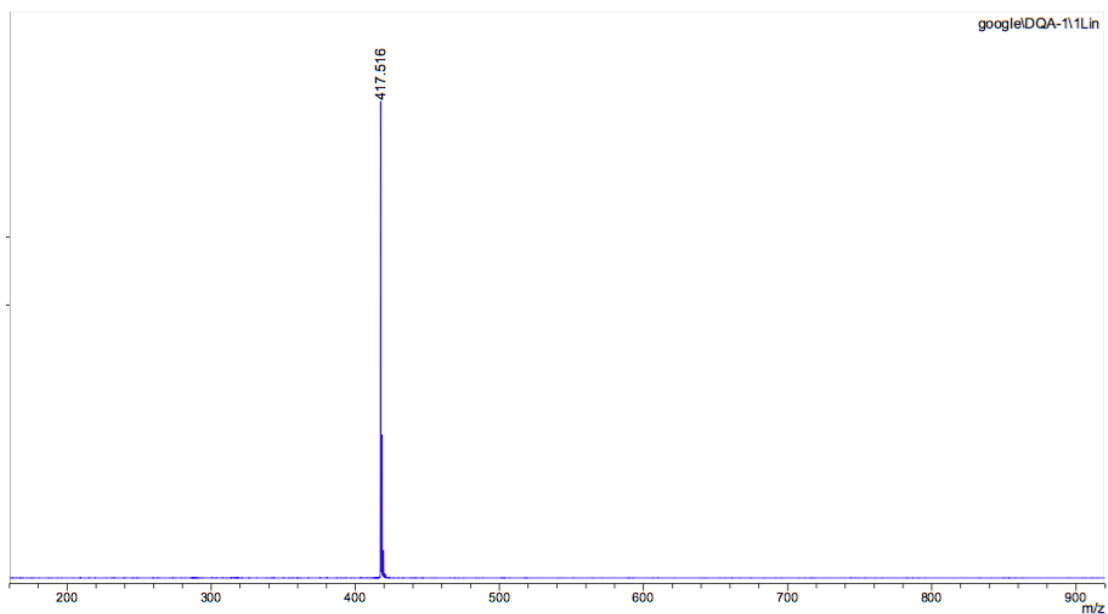Figure A.10 ^{13}C NMR of **Q3** in CDCl$_3$

Figure A.11 Mass spectrum of **Q3** *obtained by MALDI-TOF*

VITA

Mr. Chakrit Yimsukanan was born on August 8th, 1989 in Bangkok, Thailand. He graduated in Bachelor Degree of Science, majoring in Chemistry from Chulalongkorn University in 2011. Since 2012, he has been a graduate student in the program of Organic Chemistry, Faculty of Science, Chulalongkorn University and complete his Master of Science Degree in 2015. During the course of study, he received the scholarship from the Development and Promotion of Science and Technology Talents Project (DPST).

He present address is 55/40 Jaroenkrong 85, Jaroenkrong Rd., Wat Phaya-Krai district, Bangkorleam, Bangkok, Thailand 10120